Sox6 were found to boost Sox9 activity in regulating *Col2a1* expression; however, the regulatory mechanism is largely unknown as well as transcription targets beyond *Col2a1* and *Agc1* (8, 14).

MicroRNAs (miRNAs)[3] are a class of short (20–23 nucleotides), non-coding RNAs generated from primary transcripts (*pri-miRNAs*) by the action of Drosha and Dicer; they negatively regulate gene expression by promoting mRNA degradation and/or repressing translation through formation of RNA-induced silencing complexes and sequence-specific interaction with primarily 3′ untranslated regions on the target mRNA (15–17). Many miRNAs have tissue- and time-specific expression patterns determined at the *pri-miRNA* transcription level (18–20). Among known miRNAs, Tuddenham *et al.* (21) showed cartilage-specific expression of miR-140 in mouse embryos. We previously found that miR-140 expression was reduced in human osteoarthritis cartilage or in response to IL-1 stimulation, and miR-140-deficient mice exhibited short stature and age-related osteoarthritis symptoms (22, 23). These observations suggest that miR-140 plays a critical role in cartilage development and homeostasis. Recent findings indicate that Sox9 promotes miR-140 expression (24, 25), although detailed regulatory mechanisms are not fully understood.

We demonstrate in this study that the proximal upstream region of miR-140 has chondrogenic promoter activity *in vivo* and that cartilage-specific expression of miR-140 is generated from its specific transcript. We also reveal that L-Sox5 and Sox6 control miR-140 expression together with Sox9 through a response element in the promoter. Furthermore, detailed analysis suggests that the DNA binding and/or transactivation ability of Sox9 in its homodimer form is boosted by L-Sox5 and Sox6. The findings provide new insights into cartilage-specific gene regulation by this Sox trio.

EXPERIMENTAL PROCEDURES

Cell Culture, Transfection, and Adenovirus Infection—The human kidney cell line 293T and primary mouse chondrocytes were cultured in DMEM with 10% FBS at 37 °C. Primary chondrocytes were prepared from mouse embryo ribs (E16.5) and digested with collagenase. The 293T cell line was transfected using FuGENE HD transfection reagent (Promega). Sox9-expressing recombinant adenovirus was prepared for mouse chondrocytes using the adenovirus expression vector kit (Takara), and infection was performed according to manufacturer's instructions.

Reverse Transcription and Quantitative PCR—Total RNA was extracted with ISOGEN (Nippon Gene) according to the manufacturer's protocol and reverse-transcribed with SuperScript II (Invitrogen) and oligo(dT). Quantitative gene expression analysis was performed via real-time PCR using TaqMan Universal Master Mix reagents and TaqMan Probes (Applied Biosystems) on an ABI PRISM® 7900HT thermal cycler (Applied Biosystems). *Col2a1* and *Actb* were measured using the mouse TaqMan probes Mm00491889_m1 and Mm00607939_m1, respectively (Applied Biosystems). Data were normalized to *Actb* gene expression for each experiment. Quantitative miRNA expression analysis was performed using the TaqMan MicroRNA reverse transcription kit and TaqMan MicroRNA assay (Applied Biosystems). miR-140 expression was measured using the TaqMan probe TM001187, and *snoRNA202* (TM001232) expression was used as an internal control to normalize differences in each sample.

Rapid Amplification of cDNA Ends (RACE)—Total RNA and mRNA were isolated from chondrocytes with TRIzol (Invitrogen) and OligotexdT30 (Takara). 5′- and 3′-RACE were performed using the GeneRace kit (Invitrogen) with region-specific primers (5′ RACE primer (5′-CGATGCAGAGGGTGCTCCAGTACCCTGTCCGTG-3′), 5′ RACE nested primer (5′-CCGTGGTTCTACCCTGTGGTAGAACAGCATGACGT-3′), 3′ RACE primer (5′-ACCCTATGGTAGGTTACGTCATGCTGTTCTACCACAGGG-3′), and 3′ RACE nested primer (5′-ACGTCATGCTGTTCTACCACAGGGTAGAACCACGG-3′).

RNA in Situ Hybridization—Whole mount and section *in situ* hybridization was performed as previously described (26). Gene-specific fragments were amplified from mouse chondrocyte cDNA by PCR with primers (*pri-miR-140*, forward 5′-TGGTGTGTGGTTCTATGCCAGC-3′ and reverse 5′-AGCCTCAAGCCAGAATTCAGG-3′; *Sox9*, forward 5′-TTGAGACCTTCGACGTCAATGAG-3′ and reverse 5′-TCTGGCCACGAGTGGCC-3′). The *Col2a1* probe sequence was described in a previous study (27).

Sox9 Conditional Knock-out Mice—In embryos with *Sox9*, conditional knock-out mice were generated as described using *CK-19 Cre* and *Col2a1 Cre* transgenic mice (4, 28).

Reporter Assay—The pGL4.12 vector (Promega), including indicated cloned genome regions, and the indicated gene expression vector were transfected into 293T cells. The *Renilla* luciferase reporter pRL-TK (Promega) was co-transfected as a control to evaluate transfection efficiency. Cells were lysed, and luciferase activity was measured with the Dual-Glo™ Luciferase Assay System (Promega). Data were normalized to *Renilla* luciferase activity for each experiment. Mutations were introduced with QuikChange® site-directed mutagenesis (Stratagene) according to the manufacturer's instructions.

Generation of miR140 Promoter-LacZ Transgenic (Tg) Mice—To generate miR-140 promoter-LacZ Tg mice, an upstream region of miR-140 was amplified by PCR from mouse genome DNA using specific transgene primers (forward, 5′-ACTGTTCAGAAGGAGACTACTCTGTC-3′; reverse, 5′-ACCGACCTCTGCTCAGCTC-3′). The amplified fragment was cloned into a vector containing the LacZ gene, and Tg BDF1 mice were generated with pronuclear injection of the transgene. Tg mice were confirmed by PCR analysis of genomic DNA using specific transgene primers (forward, 5′-GGTGCTTTGTGAAGGGAAAG-3′; reverse, 5′-GTTGCACCACAGATGAAACG-3′).

X-Gal Staining—LacZ expression from miR140-LacZ Tg mice was detected by X-gal staining. Whole mount Tg embryos were incubated in fixation solution (1% paraformaldehyde, 0.2% glutaraldehyde, and 0.02% Nonidet P-40 in PBS) for 30 min at room temperature. The embryos were then washed with

[3] The abbreviations used are: miRNA, microRNA; RACE, rapid amplification of cDNA ends; Tg, Transgenic; TSS, transcriptional start site; PSB, putative Sox binding.

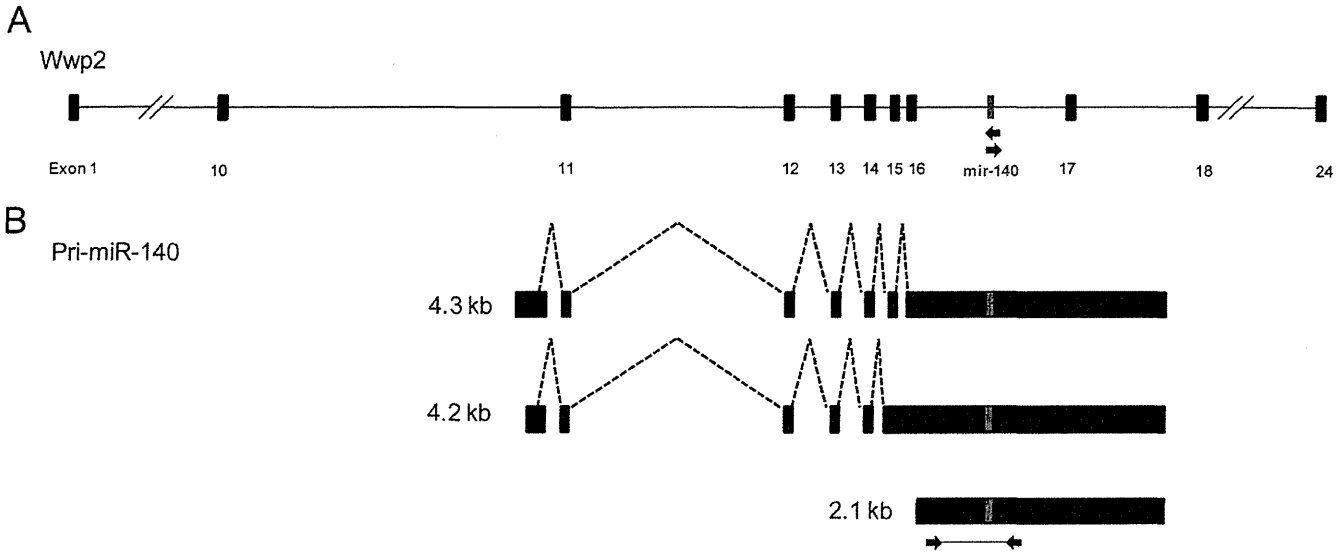

FIGURE 1. **Three isoforms were detected for *pri-miR-140*.** *A*, miR-140 is located on chromosome 8 and intron 16 of the WW domain containing E3 ubiquitin protein ligase 2 (*Wwp2*) gene. *B*, three different-sized transcripts were identified for *pri-miR-140* from 5′- and 3′-RACE performed using the primers indicated with *arrows* in *A*. The *pri-miR-140* probe used for *in situ* hybridization is indicated with *arrows* in *B*.

1 mM $MgCl_2$ in PBS and stained with staining solution (0.01% sodium deoxycholate, 0.02% Nonidet P-40, 1 mM $MgCl_2$, 5 mM potassium ferricyanide, 5 mM potassium ferrocyanide, and 0.1% X-gal in PBS) overnight at 37 °C.

Electrophoretic Mobility Shift Assay (EMSA)—DNA-protein binding was assayed with DNA probes ^{32}P-radiolabeled by end-filling with Klenow fragment and luciferase or Sox9 with or without anti-Sox9 antibodies. Reactions were carried out at 25 °C for 30 min in binding buffer (20 mM HEPES (pH 7.9),10% glycerol, 50 mM KCl, 0.05% Nonidet P-40, 0.5 mM EDTA, 0.5 mM DTT, and 1 mM PMSF) and 0.5 μg of poly(dG-dI), a non-specific competitor. Anti-Sox9 antibody was preincubated with Sox9 for 30 min at 25 °C before the addition of the radiolabeled probes. Binding reactions were separated by PAGE on a 4% gel for 3 h at 100 V. Proteins were synthesized *in vitro* with the TNT T7 Quick Coupled Transcription/Translation System (Promega) and each expression plasmid.

Chromatin Immunoprecipitation (ChIP)—ChIP was performed as previously described (29). Briefly, cells were cross-linked with 1% formaldehyde for 15 min at room temperature before glycine was added for a final concentration of 0.125 M. Chromatin was sheared to ~200–1000 bp by sonication. The chromatin solution was then incubated with the indicated antibodies bound to Dynabeads® Protein A (Dynal Biotech) at 4 °C. Sox9 (Millipore), Sox5 (Abcam, ab94396), and Sox6 (Abcam, ab30455) antibodies were used, with normal rabbit IgG antibodies (Santa Cruz Biotechnology, Inc.) as negative controls. Immune complexes were eluted from the beads and reverse-cross-linked at 65 °C. Chromatin-immunoprecipitated DNA was purified using the MinElute PCR purification kit (Qiagen) and analyzed with whole cell extract by real-time PCR with specific primers (miR140-PSB, forward 5′-GTATTTGCACA-AGGCTGGAC-3′ and reverse 5′-AGACCTGGCTGGCTC-CAT3′; miR140-Far Ups, forward 5′-CTATCTACC-CGGGCCACCTG-3′ and reverse 5′-GGACCTATGC-TGGGACAATC-3′).

RESULTS

Chondrogenic Expression of miR-140 Is Regulated by Sox9—miR-140 is located in intron 16 of the WW domain containing E3 ubiquitin protein ligase 2 (*Wwp2* gene) and consists of an N-terminal C2 domain, a C-terminal HECT domain, and four WW domains in the center (Fig. 1*A*). To determine the transcriptional start site (TSS) and 3′ end of *pri-miR-140*, we performed 5′- and 3′-RACE using mRNA from cultured mouse chondrocytes. We detected three different transcripts with the miR-140 sequence (Fig. 1*B*). The shortest was 2.1 kb long, starting inside intron 16. The two longer transcripts were splice variants 4.2 and 4.3 kb long, with the same TSS inside intron 10. All three isoforms had the same 3′ end.

miR-140 expression has been previously detected in the primordia of future bones and across the autopod, zeugopod, and stylopod of E11.5 mouse embryo forelimbs and hind limbs with a mature miR-140 LNA oligonucleotide probe (21). Still, precise temporal and spatial miR-140 expression patterns have not been characterized during chondrogenesis. To explore miR-140 expression further, we performed *in situ* hybridization using an RNA probe for *pri-miR-140* common to all three isoforms (Fig. 1*B*). The expression pattern in the cartilage of E11.5 embryos was similar to the chondrocyte differentiation markers *Sox9* and *Col2a1*, a target gene of Sox9 (Fig. 2, *A–F*). *Sox9* and miR-140 expressions were also similarly detected in the cartilage of digits from E11.5 to E14.5 (Fig. 2, *G* and *H*).

Our *in situ* hybridization analysis found that miR-140 expression resembled *Sox9* and one of its target genes, *Col2a1* expression in limb buds, which suggests the possibility that Sox9 regulates miR-140 expression in limb development. To test this hypothesis, we examined the effect of repressing Sox9 expression on miR-140 expression. *Sox9flox/flox;Ck19-Cre* embryos abolish Sox9 expression before mesenchymal condensation, and chondrogenic cell lineage commitment is profoundly impaired as a consequence (28). In E12.5 wild type and

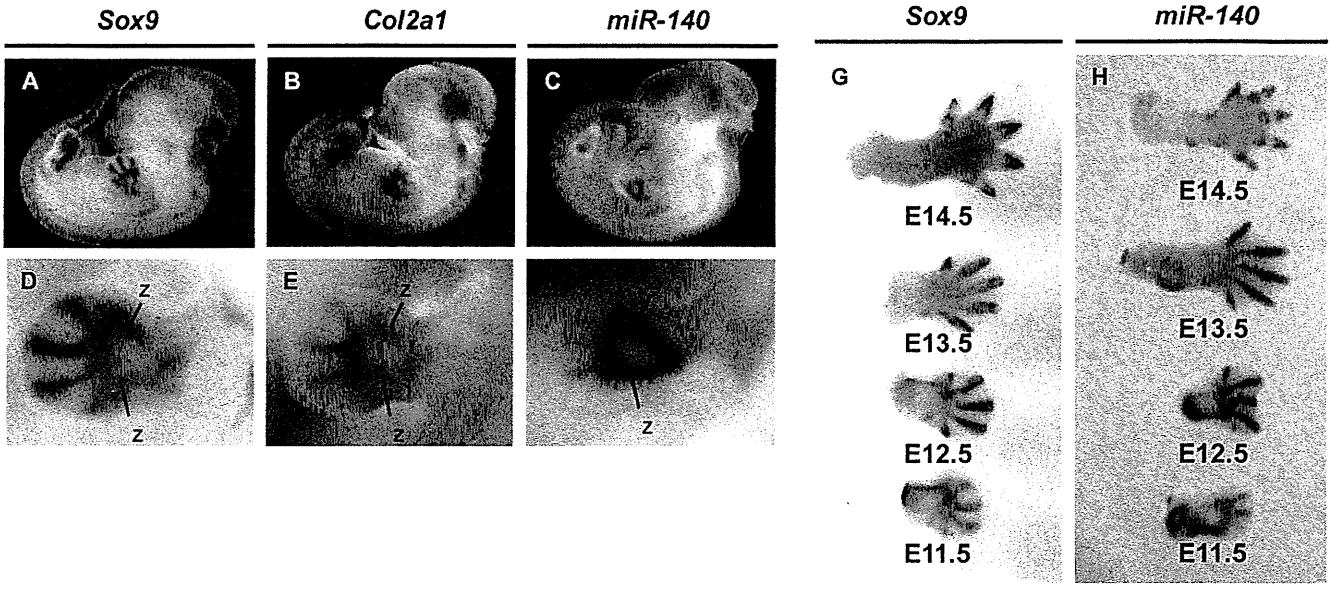

FIGURE 2. **Cartilage-specific expression of *pri-miR-140* in mouse embryos.** Shown is a comparison of *Sox9* (*A* and *D*), *Col2a1* (*B* and *E*), and *pri-miR-140* (*C* and *F*) expression patterns in mouse whole mount embryos and developing mouse forelimb buds at embryonic stage E11.5. Zeugopod elements are indicated as *z*. Shown is the Sox9 (*G*) and *Pri-miR-140* (*H*) expression pattern in the cartilage of developing digits during E11.5 to E14.5.

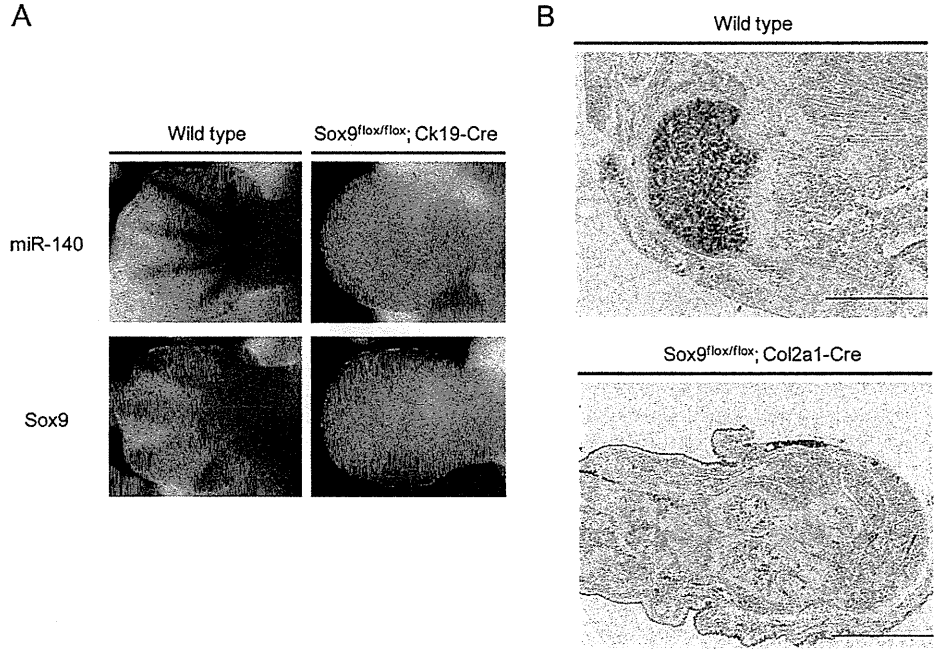

FIGURE 3. **Pri-miR-140 expression is reduced in Sox9-deficient mouse limb buds and chondrocytes.** *A*, *Pri-miR-140* and Sox9 expression patterns in the forelimb buds of wild type and *Sox9flox/flox;Ck19-Cre* mouse embryos at E12.5 are shown. Expression of both transcripts was drastically reduced in mutant embryos. *B*, *Pri-miR-140* expression was detected in wild type femurs at E16.5 but not E16.5 *Sox9flox/flox;Col2a1-Cre* femurs.

Sox9flox mice without Cre expression, the miR-140 expression pattern overlapped with the Sox9 pattern (Fig. 3*A*, *left*). Expression of *pri-miR-140* in Sox9 mutant cells at E12.5 was completely absent, however, as was Sox9 expression (Fig. 3*A*, *right*). These results suggest that Sox9 is a regulator of miR-140, but there is a possibility that the absence of miR-140 expression in the *Sox9flox/flox;Ck19-Cre* embryo limb buds was the result of absent chondrogenic lineage cells from impaired chondrogenic mesenchymal condensation. We thus examined *Sox9flox/flox; Col2a1-Cre* embryos, where Sox9 was inactivated in condensed mesenchymal cells and differentiated chondrocytes through *Col2a1-Cre*-mediated recombination (4). In E16.5 wild type embryos, *pri-miR-140* was expressed in the proliferating chondrocyte zone but absent in the hypertrophic zone (Fig. 3*B*, *top*). In contrast, miR-140 was completely absent in condensed chondrogenic mesenchymal cells and differentiated chondrocytes from *Sox9flox/flox; Col2a1-Cre* embryos (Fig. 3*B*, *bottom*). This shows that Sox9 dominates regulation of miR-140 expression in differentiating chondrocytes *in vivo*.

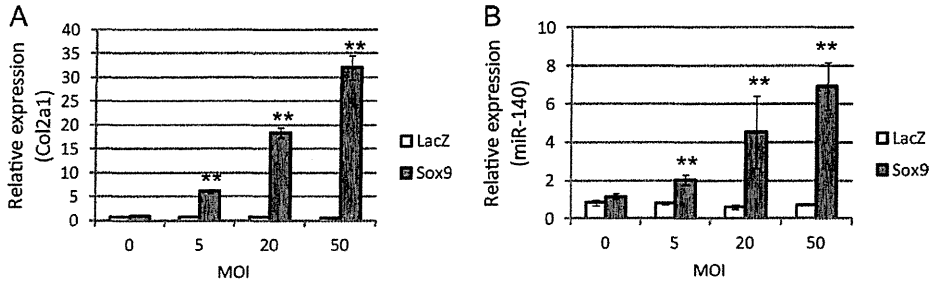

FIGURE 4. **miR-140 expression is up-regulated by Sox9 in chondrocytes.** LacZ-expressing adenoviruses as a negative control or Sox9-expressing adenoviruses were transduced into cultured mouse chondrocytes with incremental multiplicities of infection (*MOI*). *Col2a1* mRNA (*A*) and miR-140 (*B*) expression after Sox9 overexpression were evaluated with quantitative PCR. Data are presented as the mean ± S.D.; $n = 3$. Statistical differences were calculated using the *t* test. **, $p < 0.01$

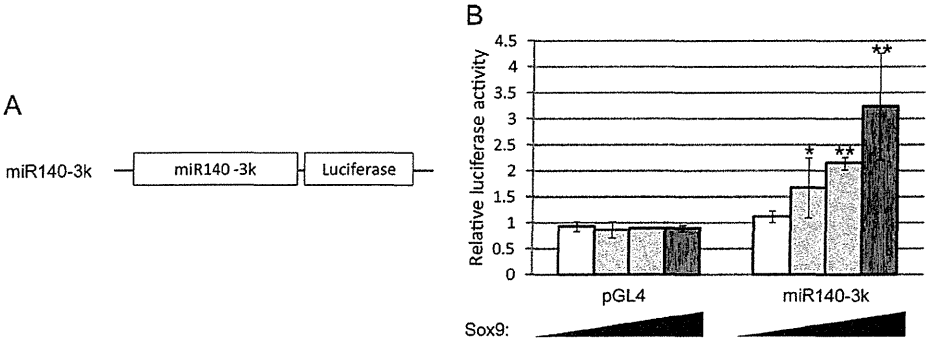

FIGURE 5. **miR-140 proximal promoter activity is up-regulated by Sox9.** *A*, shown is a luciferase reporter construct containing a 3-kb proximal upstream region of *pri-miR-140*. *B*, 293T cells were co-transfected with pGL4 as a negative control or the miR140–3k reporter plasmid and increasing amounts of Sox9-expressing plasmid (0, 50, 100, and 400 ng). Luciferase activity is presented as the mean ± S.D.; $n = 3$. Statistical differences were calculated using *t* test. *, $p < 0.05$; **, $p < 0.01$.

We also studied the effect of Sox9 overexpression on miR-140 expression through quantitative PCR analysis for cultured chondrocytes. Adenovirus infection-mediated Sox9 overexpression increased miR-140 expression as well as *Col2a1* expression and correlated with increased multiplicity of infection; adenovirus infection-mediated LacZ overexpression did not affect miR-140 expression (Fig. 4, *A* and *B*). Taken together, the results from all these experiments indicate that miR-140 expression is up-regulated by Sox9 in chondrocytes and developing limbs.

Upstream Region of miR-140 Is Critical for Its Chondrogenic Expression and Sox9 Regulation—To determine a direct regulatory mechanism for miR-140 expression by Sox9, we constructed a reporter plasmid with a 3-kb region upstream from the miR-140 TSS and a luciferase gene (miR140–3k). With the reporter plasmid and increasing amounts of Sox9-expressing plasmids, luciferase activity in 293T cells increased in a dose-dependent manner (Fig. 5). Sox9 thus regulates miR-140 expression by activating a promoter region 3 kb upstream of its TSS.

Another reporter plasmid with the 3-kb region upstream of miR-140 and a *LacZ* gene (Fig. 6*A*) was prepared and used to generate transgenic (Tg) mice (miR140–3k-LacZ). We generated three lines of transgenic mice, and all of those transgenic E12.5 and E15.5 embryos revealed LacZ expression in forelimbs, hind limbs, and other cartilage tissue such as ribs and vertebrae with an expression pattern similar to miR-140 (Fig. 6, *B–E*). These *in vitro* and *in vivo* results suggest that miR-140 expression in limb development and cartilaginous tissues is regulated by a 3-kb region upstream of its TSS and promoted by Sox9.

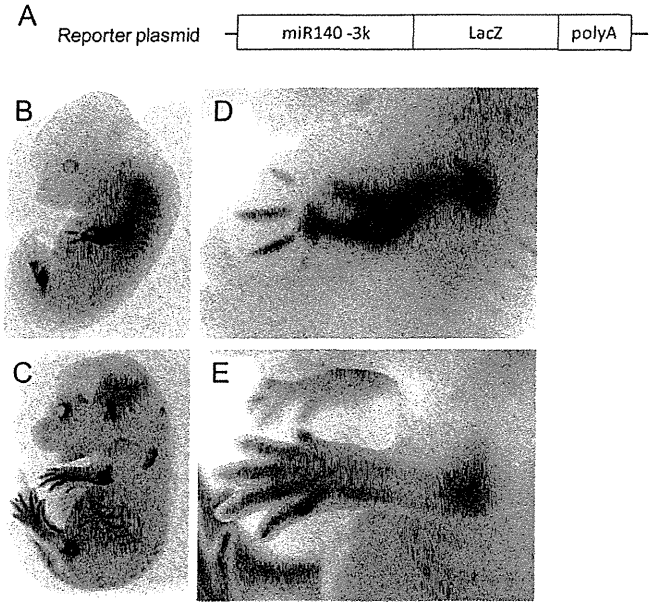

FIGURE 6. **The miR-140 proximal promoter has chondrogenic activity.** *A*, shown is an LacZ construct containing a 3-kb upstream region of *pri-miR-140* transgene. LacZ expression patterns in miR140–3k-LacZ transgenic (Tg) mouse embryos at E12.5 (*B*) and E15.5 (*C*). Shown is a magnified view of forelimb at E12.5 (*D*) and E15.5 (*E*).

Sox9 Binds to Upstream Region of miR-140 and Enhances Its Expression in Concert with L-Sox5 and Sox6—Previous studies have clarified that L-Sox5 and Sox6 are critical regulators of

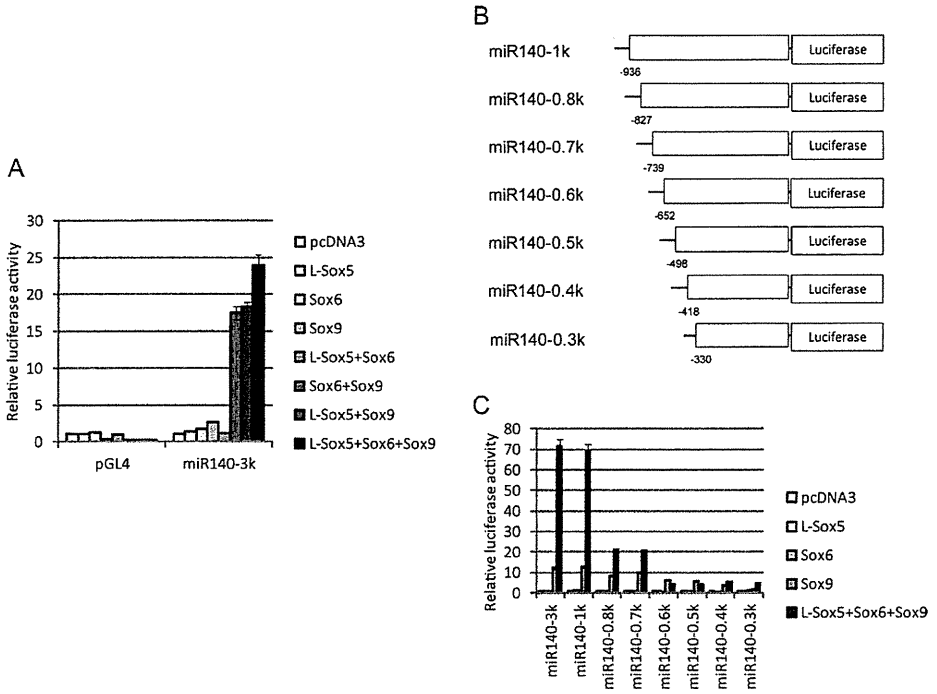

FIGURE 7. **L-Sox5 and Sox6 enhance Sox9-dependent proximal promoter activation of miR-140.** *A*, 293T cells were co-transfected with pGL4 as a negative control or with the miR140–3k reporter plasmid and the indicated expression plasmids. Luciferase activity is presented as the mean ± S.D.; $n = 3$. *B*, luciferase reporter constructs containing different lengths of the miR-140 upstream region are shown. *Numbers* indicate position from the *pri-miR-140* transcription start site. *C*, luciferase activity using the reporter plasmids displayed in *B* and indicated expressing plasmids is presented as the mean ± S.D.; $n = 3$.

chondrogenesis and function as Sox9 co-operators in chondrocytes (4, 14). It has also been reported that expression of chondrogenic genes regulated by Sox9, such as *Col2a1* and *Agc1*, is enhanced by L-Sox5 and Sox6 (8, 14). Therefore, we explored whether L-Sox5 and Sox6 were involved with Sox9 in regulation of miR-140 expression.

We first examined promoter activity from the miR140–3k reporter plasmid coupled with overexpression of L-Sox5, Sox6, and/or Sox9 in 293T cells. Luciferase activity was greater with overexpression of the Sox trio than with Sox9 alone, and L-Sox5 and/or Sox6 did not enhance activity without Sox9 overexpression (Fig. 7*A*). L-Sox5 and Sox6 can thus promote miR-140 expression through activating Sox9.

A series of deletion constructs in the miR-140 upstream region was then created to identify the Sox trio response element (Fig. 7*B*). Luciferase activity up-regulated by the Sox trio decreased with a deletion from −936 to −827 bp upstream of the miR140 TSS and was almost abolished with a deletion from −739 to −652 bp (Fig. 7*C*). Remarkably, an additional increase in activity by L-Sox5 and Sox6 co-transfected with Sox9 was not shown with deletion of the −739 to −652 bp upstream region (Fig. 7*C*).

Our luciferase assay analysis indicates that the −739 bp upstream region from miR-140 TSS is minimally required for its regulation by L-Sox5, Sox6, and Sox9 (Sox trio). We then constructed a LacZ reporter plasmid containing −739 bp upstream region from miR-140 TSS (Fig. 8*A*) and generated Tg mice (miR140–0.7k-LacZ) to examine whether the minimal region is essential for its chondrogenic expression. We observed that the four other miR140–0.7k-LacZ mice expressed LacZ in cartilaginous tissues that expression was similar to

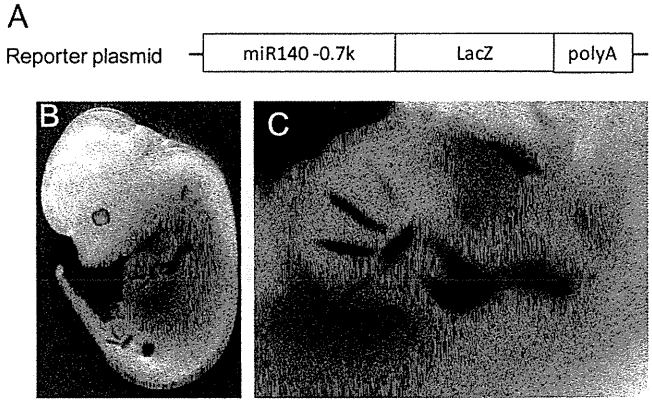

FIGURE 8. **The 0.7-kb upstream region of miR-140 has chondrogenic promoter activity.** *A*, shown is the LacZ reporter construct containing −739 bp upstream region of *pri-miR-140* transgene. *B*, shown are LacZ expression patterns in miR140–0.7k-LacZ Tg mouse of E12.5 embryos. *C*, shown is a magnified view of forelimb.

miR140–3k-LacZ mice (Fig. 8, *B* and *C*). These results indicate that the −739-bp proximal upstream region of miR-140, which is minimally required for its regulation by Sox trio, is essential for its chondrogenic expression.

The −739 to −652-bp upstream region was then explored in detail because up-regulation by the Sox trio was abolished with its deletion. We looked for consensus Sox9 binding sequences because Sox trio up-regulation was still Sox9-dependent and found a putative imperfect palindromic sequence in the binding site (Fig. 9*A*). Previous reports indicated that Sox9 homodimers bind to enhancer regions that contain inverted Sox9 binding sites separated by 3–4 bp and represent a palindromic motif for chondrocyte-specific gene regulation (30–32). To assess

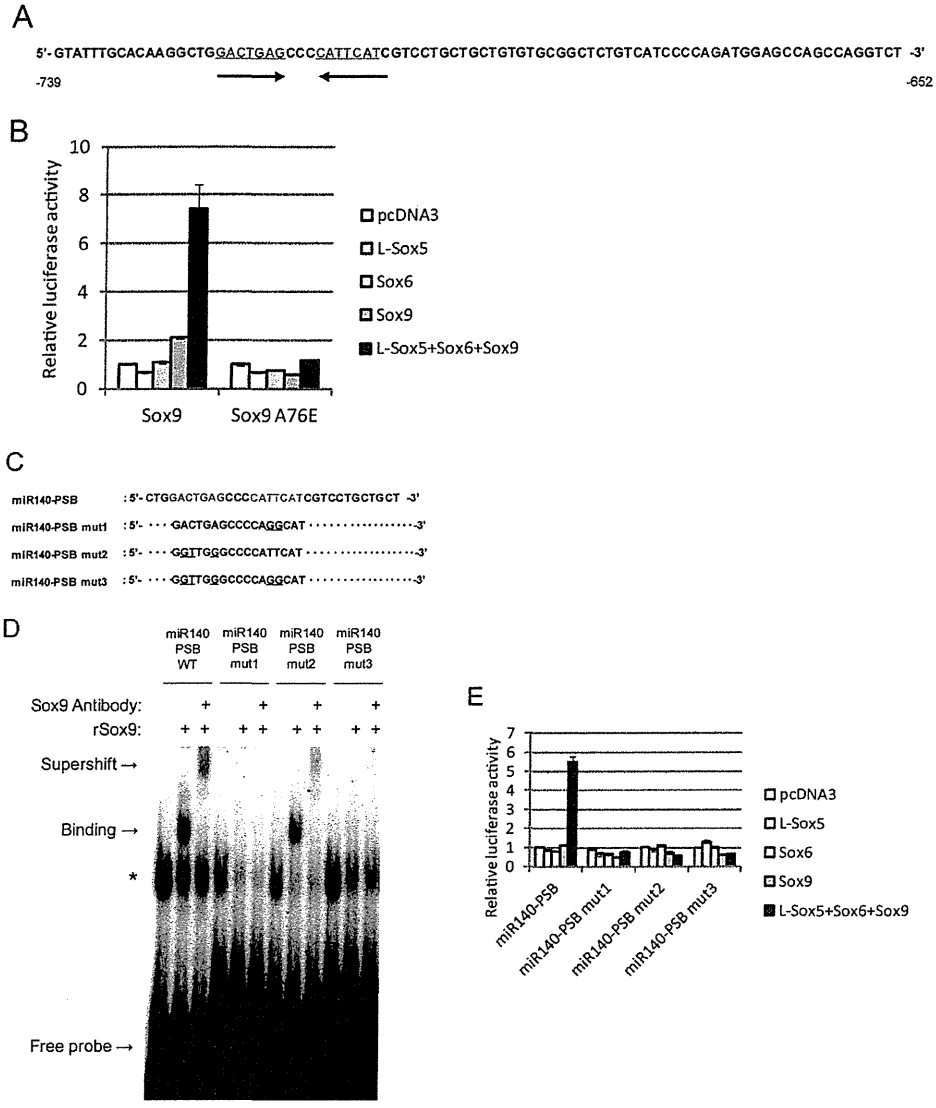

FIGURE 9. **The L-Sox5 and Sox6 cooperative effect for miR-140 promoter activation is repressed by blockage of Sox9 homodimer formation.** *A*, shown is a sequence of the region −739 and −652 bp upstream from the *pri-miR-140* transcription start site. A putative Sox9 binding site is indicated in *red*; *arrows* indicate site orientation. *B*, 293T cells were co-transfected with the miR140−0.7k reporter plasmid displayed in Fig. 7*B* and the indicated expressing plasmids. Wild type Sox9 (*left*) or Sox9 with a dimerization missense mutation (A76E) (*right*) were used as expression plasmids. Luciferase activity is presented as the mean ± S.D.; $n = 3$. *C*, shown are wild type and mutant oligonucleotide probe sequences corresponding to Sox9 binding sites in the miR-140 promoter. *D*, binding of oligonucleotide probes with wild type and mutated PSB consensus sequences complexed to recombinant Sox9 protein (*rSox9*) was detected by electrophoretic mobility shift assay. Mutations in one (*mut1*, *mut2*) or both (*mut3*) Sox9 binding motifs were compared with the wild type (*WT*) in the presence or absence of anti-Sox9 antibody. *E*, 293T cells were co-transfected with reporter plasmids containing the −739- and −652-bp *pri-miR-140* wild type upstream region (*miR140-PSB*) or the mutations displayed in C and the indicated expressing plasmids. Luciferase activity is presented as the mean ± S.D.; $n = 3$.

whether Sox9 homodimer binding was critical for miR-140 regulation, a miR140−0.7k reporter construct and Sox9 A76E expression plasmid that does not form homodimers were used (30–32). There was no obvious up-regulation of luciferase activity by Sox9 A76E alone or with co-expression in the Sox trio, in contrast to the Sox9 wild type plasmid (Fig. 9*B*). To confirm that Sox9 binds to the putative palindromic sequence, we performed EMSA using oligonucleotide probes for the putative Sox binding (PSB) sequences (Fig. 9*C*). miR140-PSB probes detected a band when incubated with recombinant Sox9 protein, and additional incubation with anti-Sox9 antibody reduced the band with an upward supershift (Fig. 9*D*). Utilizing probes with point mutations in one or both Sox9 binding sequences (Fig. 9*C*) resulted in band reduction, where miR140-PSB mut1 almost abolished the band, and mutations in both motif sites completely abolished the band (Fig. 9*D*). The same results occurred with the supershift band produced by incubation with anti-Sox9 antibody (Fig. 9*D*). To further confirm Sox9 binding and promoter activity in the −739 ~ −652-bp region upstream of the miR-140 TSS, another luciferase reporter assay was performed with a vector containing point mutations in one or both Sox9 motif sites. Dual mutations and a single Sox9 motif mutation diminished up-regulation of promoter activity by Sox trio expression (Fig. 9*E*).

Finally, the ability of Sox9 to bind to the endogenous miR-140 promoter was examined in E13.5 mouse limbs by a ChIP

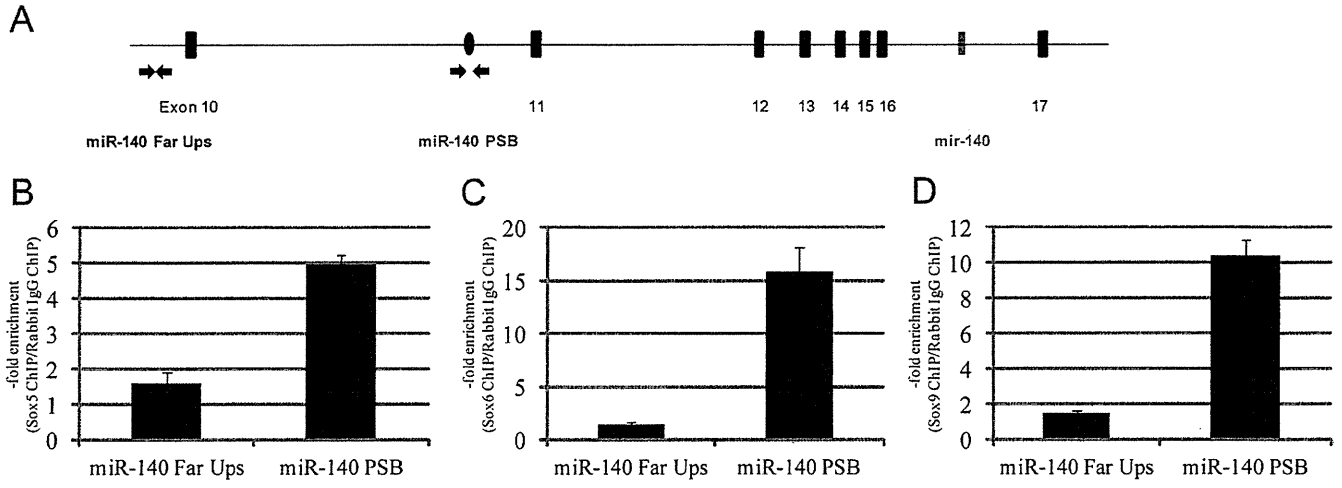

FIGURE 10. **The Sox trio binds to the miR-140 promoter in E13.5 mouse limbs.** *A*, location of site-specific primer sets for PSB sites and the −5 kb upstream (*Far Ups*) region of the *pri-miR-140* TSS as a negative control are displayed by *arrows*. *B*, chromatin-immunoprecipitated DNA and whole cell extract DNA in E13.5 mouse limbs were quantitatively analyzed by real-time PCR. The enrichment value of L-Sox5 (*B*), Sox6 (*C*), and Sox9 (*D*) chromatin-immunoprecipitated DNA was calculated by dividing rabbit IgG chromatin-immunoprecipitated DNA data as a negative control. Data are presented as the mean ± S.D.; $n = 3$.

assay using far upstream (approximately −5 kb) (miR140 Far Ups) and putative Sox9 binding site (miR140 PSB) primer sets as shown in Fig. 10*A*. The enrichment value of the putative Sox9 binding site was confirmed in Sox9 chromatin-immunoprecipitated DNA, although the far upstream site did not show enrichment (Fig. 10*B*). Additionally, the use of antibodies showed that L-Sox5 and Sox6 also bound to the putative Sox9 binding site but not the far upstream site (Fig. 10, *C* and *D*). Taken together, these results suggest that Sox9 enhances miR-140 expression by cooperating with L-Sox5 and Sox6 to bind −739 ~ −652 bp upstream from the miR-140 TSS.

DISCUSSION

Most miRNAs, which frequently are located within the intron region of genes, originate from the spliced intronic RNA of a host gene transcript (33). The cartilage-specific intronic miRNA miR-140 is located in intron 16 of *Wwp2*, a host gene that functions as a critical regulator of craniofacial development and is also expressed in cartilaginous tissues (34, 35). *Wwp2* expression is directly regulated by the binding of Sox9 to intron 3 (35), which suggests that miR-140 expression can be similarly generated and regulated from the *Wwp2* transcript. In this study we demonstrated that the proximal upstream region of *pri-miR-140* located in intron 10 of *Wwp2* has *in vivo* promoter activity. The results suggest that miR-140 may be derived from its own specific transcript during chondrogenesis.

Previous studies found miR-140 to be specifically expressed in chondrocytes and a critical regulator of cartilage development and homeostasis (21–23). Our *in situ* hybridization analysis confirmed that *pri-miR-140* expression was chondrocyte-specific in mouse embryos and mirrored Sox9 expression patterns as shown in limb buds. Also, miR-140 expression was abolished in Sox9-deficient limb buds and chondrocytes and enhanced in cultured chondrocytes with overexpressed Sox9. These findings show that Sox9 is a direct regulator of miR-140 as well as *Wwp2*. A recent study indicated that Sox9 binds to intron 10 of *Wwp2* and up-regulates miR-140 expression (25). By further exploring this mechanism, we found that Sox9 activates a promoter region upstream of miR-140 on intron 10 with *in vivo* chondrogenic activity. This strongly suggests that miR-140 *in vivo* chondrogenic expression is directly regulated in part through activation of its promoter region by Sox9 instead of splicing itself out of the host transcript.

Most previously known Sox9 targets were extracellular matrix genes, and only a few, such as *Bapx1*, *S100A1*, and *S100B*, were shown to be direct regulators of it except for extracellular matrix genes (29, 36). Our *in vivo* and *in vitro* analyses demonstrated that miR-140 is also a downstream target of Sox9. Previous studies reported that miR-140 repressed Hdac4 to block chondrocyte maturation, Adamts-5 to promote cartilage development and homeostasis, and Sp1 to maintain chondrocyte proliferation (21, 23, 25). These diverse roles are similar to Sox9, which also promotes early chondrogenesis but represses chondrocyte maturation (2). Furthermore, Sox9 expression was significantly lower in osteoarthritis cartilage compared with normal cartilage (37), whereas miR-140 knockout mice exhibited age-related, osteoarthritis-like phenotypes (23). These studies strongly support miR-140 as both a downstream and a critical target of Sox9 due to its diverse roles in chondrogenesis. In fact, miR-140-deficient mice have a mild skeletal phenotype with a short stature (23).

In this study we showed that L-Sox5 and Sox6 were also involved in regulation of miR-140 expression with Sox9. Results showed that expression levels did not change in the presence of L-Sox5 and/or Sox6 without Sox9 co-expression, making control of miR-140 expression by L-Sox5 and Sox6 completely Sox9-dependent. L-Sox5 and Sox6 participate in the regulation of cartilage-specific genes such as *Col2a1* and *Agc1*, although they have no known transactivation or transrepression domains (8, 14). A recent study suggested that L-Sox5 and Sox6 may facilitate Sox9 DNA binding by an unknown mechanism (8). A comparable regulatory event by the Sox trio may also occur with the miR-140 promoter.

Our detailed luciferase, EMSA, and ChIP analyses identified the precise Sox trio response element and Sox9 binding site.

Sox9 was previously reported as bound to intron 10 of *Wwp2* to regulate miR-140 expression (25). However, the Sox9 binding site exhibited in this study is different and suggests the possibility that miR-140 expression is controlled by multiple Sox9 and/or the Sox trio binding in its promoter region, as shown with *Col11a2* expression that is directed by Sox9 at least three cartilage-specific enhancer elements (38).

Sox9 is critical to chondrogenesis because it regulates cartilage-specific genes such as *Col2a1*, *Col11a2*, and *Agc1* (7, 10, 11). In addition, Sox9 plays a critical role in testicular development by regulating targets such as *Amh* and *Ptgds* in Sertoli cells (39–41). However, the regulatory mechanism of tissue-specific target distribution is less understood. Previous reports indicated a human SOX9 missense mutation (A76E) in an XY patient exhibiting skeletal abnormalities without sex reversal; this mutation perturbed Sox9 dimerization, resulting in dysregulation of chondrocyte-specific genes (30–32). Sox9 homodimers are believed to bind to enhancer regions containing inverted Sox9 binding sites separated by 3 or 4 bp (30–32). The Sox9 binding site identified in this study is also a Sox9 palindromic binding motif and again indicates that miR-140 is a critical chondrocyte-specific target. In fact, LacZ expression was not detected in the male gonads of any miR140–3k-LacZ Tg embryonic mice (data not shown). We further showed that Sox9 A76E did not up-regulate miR-140 promoter activity even when L-Sox5 and Sox6 were co-expressed. Only one site mutation of the Sox9 palindromic motif completely abolished the ability of the Sox trio to up-regulate promoter activity despite a Sox9 motif mutation that decreased but retained Sox9 binding status. These findings suggest that DNA-dependent Sox9 homodimer formation is needed for L-Sox5 and Sox6 assembly to enhance its DNA binding and/or transactivation ability, but a more detailed mechanism remains undetermined. As previously mentioned, binding of the Sox9 homodimer to its palindromic motif is critical for cartilage-specific gene regulation, and the regulatory mechanism suggested in this study could apply to other cartilage targets. In fact, we observed that Sox9 A76E did not up-regulate luciferase activity from a *Col2a1* enhancer reporter vector with L-Sox5 and Sox6 co-transfection (data not shown).

In conclusion, we report that a proximal region upstream of miR-140 has chondrogenic promoter activity *in vivo*, and its cartilage-specific expression is generated from its transcript within the host gene *Wwp2*. miR-140 promoter activity is up-regulated by the critical transcription factors L-Sox5, Sox6, and Sox9, and their response elements and detailed binding sites were identified. Our findings suggest that the DNA binding and/or transactivation ability of Sox9 in its homodimer form is dependently boosted by L-Sox5 and Sox6.

Acknowledgments—We thank Dr. Makoto Taketo of Kyoto University for the Ck19-Cre mice. We thank Akane Nakamura and Hideki Tsumura for help with generation of miR140–3k-LacZ transgenic mice and Arisa Igarashi and Moe Tamano for technical assistance.

REFERENCES

1. Provot, S., and Schipani, E. (2005) Molecular mechanisms of endochondral bone development. *Biochem. Biophys. Res. Commun.* **328,** 658–665
2. Lefebvre, V., and Smits, P. (2005) Transcriptional control of chondrocyte fate and differentiation. *Birth Defects Res. C Embryo Today* **75,** 200–212
3. Goldring, M. B., Tsuchimochi, K., and Ijiri, K. (2006) The control of chondrogenesis. *J. Cell. Biochem.* **97,** 33–44
4. Akiyama, H., Chaboissier, M. C., Martin, J. F., Schedl, A., and de Crombrugghe, B. (2002) The transcription factor Sox9 has essential roles in successive steps of the chondrocyte differentiation pathway and is required for expression of Sox5 and Sox6. *Genes Dev.* **16,** 2813–2828
5. Akiyama, H., Lyons, J. P., Mori-Akiyama, Y., Yang, X., Zhang, R., Zhang, Z., Deng, J. M., Taketo, M. M., Nakamura, T., Behringer, R. R., McCrea, P. D., and de Crombrugghe, B. (2004) Interactions between Sox9 and β-catenin control chondrocyte differentiation. *Genes Dev.* **18,** 1072–1087
6. Bi, W., Deng, J. M., Zhang, Z., Behringer, R. R., and de Crombrugghe, B. (1999) Sox9 is required for cartilage formation. *Nat. Genet.* **22,** 85–89
7. Bridgewater, L. C., Lefebvre, V., and de Crombrugghe, B. (1998) Chondrocyte-specific enhancer elements in the Col11a2 gene resemble the Col2a1 tissue-specific enhancer. *J. Biol. Chem.* **273,** 14998–15006
8. Han, Y., and Lefebvre, V. (2008) L-Sox5 and Sox6 drive expression of the aggrecan gene in cartilage by securing binding of Sox9 to a far-upstream enhancer. *Mol. Cell. Biol.* **28,** 4999–5013
9. Kou, I., and Ikegawa, S. (2004) SOX9-dependent and -independent transcriptional regulation of human cartilage link protein. *J. Biol. Chem.* **279,** 50942–50948
10. Lefebvre, V., Huang, W., Harley, V. R., Goodfellow, P. N., and de Crombrugghe, B. (1997) SOX9 is a potent activator of the chondrocyte-specific enhancer of the pro-α1(II) collagen gene. *Mol. Cell. Biol.* **17,** 2336–2346
11. Sekiya, I., Tsuji, K., Koopman, P., Watanabe, H., Yamada, Y., Shinomiya, K., Nifuji, A., and Noda, M. (2000) SOX9 enhances aggrecan gene promoter/enhancer activity and is up-regulated by retinoic acid in a cartilage-derived cell line, TC6. *J. Biol. Chem.* **275,** 10738–10744
12. Xie, W. F., Zhang, X., Sakano, S., Lefebvre, V., and Sandell, L. J. (1999) Trans-activation of the mouse cartilage-derived retinoic acid-sensitive protein gene by Sox9. *J. Bone Miner. Res.* **14,** 757–763
13. Smits, P., Li, P., Mandel, J., Zhang, Z., Deng, J. M., Behringer, R. R., de Crombrugghe, B., and Lefebvre, V. (2001) The transcription factors L-Sox5 and Sox6 are essential for cartilage formation. *Dev. Cell* **1,** 277–290
14. Lefebvre, V., Li, P., and de Crombrugghe, B. (1998) A new long form of Sox5 (L-Sox5), Sox6, and Sox9 are coexpressed in chondrogenesis and cooperatively activate the type II collagen gene. *EMBO J.* **17,** 5718–5733
15. Bartel, D. P. (2009) MicroRNAs. Target recognition and regulatory functions. *Cell* **136,** 215–233
16. Cai, X., Hagedorn, C. H., and Cullen, B. R. (2004) Human microRNAs are processed from capped, polyadenylated transcripts that can also function as mRNAs. *RNA* **10,** 1957–1966
17. Lee, Y., Kim, M., Han, J., Yeom, K. H., Lee, S., Baek, S. H., and Kim, V. N. (2004) MicroRNA genes are transcribed by RNA polymerase II. *EMBO J.* **23,** 4051–4060
18. Liu, N., Williams, A. H., Kim, Y., McAnally, J., Bezprozvannaya, S., Sutherland, L. B., Richardson, J. A., Bassel-Duby, R., and Olson, E. N. (2007) An intragenic MEF2-dependent enhancer directs muscle-specific expression of microRNAs 1 and 133. *Proc. Natl. Acad. Sci. U.S.A.* **104,** 20844–20849
19. Rao, P. K., Kumar, R. M., Farkhondeh, M., Baskerville, S., and Lodish, H. F. (2006) Myogenic factors that regulate expression of muscle-specific microRNAs. *Proc. Natl. Acad. Sci. U.S.A.* **103,** 8721–8726
20. Zhao, Y., Samal, E., and Srivastava, D. (2005) Serum response factor regulates a muscle-specific microRNA that targets Hand2 during cardiogenesis. *Nature* **436,** 214–220
21. Tuddenham, L., Wheeler, G., Ntounia-Fousara, S., Waters, J., Hajihosseini, M. K., Clark, I., and Dalmay, T. (2006) The cartilage specific microRNA-140 targets histone deacetylase 4 in mouse cells. *FEBS Lett.* **580,** 4214–4217
22. Miyaki, S., Nakasa, T., Otsuki, S., Grogan, S. P., Higashiyama, R., Inoue, A., Kato, Y., Sato, T., Lotz, M. K., and Asahara, H. (2009) MicroRNA-140 is expressed in differentiated human articular chondrocytes and modulates interleukin-1 responses. *Arthritis Rheum.* **60,** 2723–2730
23. Miyaki, S., Sato, T., Inoue, A., Otsuki, S., Ito, Y., Yokoyama, S., Kato, Y., Takemoto, F., Nakasa, T., Yamashita, S., Takada, S., Lotz, M. K., Ueno-Kudo, H., and Asahara, H. (2010) MicroRNA-140 plays dual roles in both

cartilage development and homeostasis. *Genes Dev.* **24,** 1173–1185
24. Nakamura, Y., He, X., Kato, H., Wakitani, S., Kobayashi, T., Watanabe, S., Iida, A., Tahara, H., Warman, M. L., Watanapokasin, R., and Postlethwait, J. H. (2012) Sox9 is upstream of microRNA-140 in cartilage. *Appl. Biochem. Biotechnol.* **166,** 64–71
25. Yang, J., Qin, S., Yi, C., Ma, G., Zhu, H., Zhou, W., Xiong, Y., Zhu, X., Wang, Y., He, L., and Guo, X. (2011) miR-140 is co-expressed with Wwp2-C transcript and activated by Sox9 to target Sp1 in maintaining the chondrocyte proliferation. *FEBS Lett.* **585,** 2992–2997
26. Yokoyama, S., Hashimoto, M., Shimizu, H., Ueno-Kudoh, H., Uchibe, K., Kimura, I., and Asahara, H. (2008) Dynamic gene expression of Lin-28 during embryonic development in mouse and chicken. *Gene Expr. Patterns* **8,** 155–160
27. Kawakami, Y., Tsuda, M., Takahashi, S., Taniguchi, N., Esteban, C. R., Zemmyo, M., Furumatsu, T., Lotz, M., Belmonte, J. C., and Asahara, H. (2005) Transcriptional coactivator PGC-1α regulates chondrogenesis via association with Sox9. *Proc. Natl. Acad. Sci. U.S.A.* **102,** 2414–2419
28. Barrionuevo, F., Taketo, M. M., Scherer, G., and Kispert, A. (2006) Sox9 is required for notochord maintenance in mice. *Dev. Biol.* **295,** 128–140
29. Yamashita, S., Andoh, M., Ueno-Kudoh, H., Sato, T., Miyaki, S., and Asahara, H. (2009) Sox9 directly promotes Bapx1 gene expression to repress Runx2 in chondrocytes. *Exp. Cell Res.* **315,** 2231–2240
30. Bernard, P., Tang, P., Liu, S., Dewing, P., Harley, V. R., and Vilain, E. (2003) Dimerization of SOX9 is required for chondrogenesis but not for sex determination. *Hum. Mol. Genet.* **12,** 1755–1765
31. Coustry, F., Oh, C. D., Hattori, T., Maity, S. N., de Crombrugghe, B., and Yasuda, H. (2010) The dimerization domain of SOX9 is required for transcription activation of a chondrocyte-specific chromatin DNA template. *Nucleic Acids Res.* **38,** 6018–6028
32. Sock, E., Pagon, R. A., Keymolen, K., Lissens, W., Wegner, M., and Scherer, G. (2003) Loss of DNA-dependent dimerization of the transcription factor SOX9 as a cause for campomelic dysplasia. *Hum. Mol. Genet.* **12,** 1439–1447
33. Baskerville, S., and Bartel, D. P. (2005) Microarray profiling of microRNAs reveals frequent coexpression with neighboring miRNAs and host genes. *RNA* **11,** 241–247
34. Nakamura, Y., He, X., Kobayashi, T., Yan, Y. L., Postlethwait, J. H., and Warman, M. L. (2008) Unique roles of microRNA140 and its host gene WWP2 in cartilage biology. *J. Musculoskelet. Neuronal Interact.* **8,** 321–322
35. Zou, W., Chen, X., Shim, J. H., Huang, Z., Brady, N., Hu, D., Drapp, R., Sigrist, K., Glimcher, L. H., and Jones, D. (2011) The E3 ubiquitin ligase Wwp2 regulates craniofacial development through mono-ubiquitylation of Goosecoid. *Nat. Cell Biol.* **13,** 59–65
36. Saito, T., Ikeda, T., Nakamura, K., Chung, U. I., and Kawaguchi, H. (2007) S100A1 and S100B, transcriptional targets of SOX trio, inhibit terminal differentiation of chondrocytes. *EMBO Rep.* **8,** 504–509
37. Haag, J., Gebhard, P. M., and Aigner, T. (2008) SOX gene expression in human osteoarthritic cartilage. *Pathobiology* **75,** 195–199
38. Bridgewater, L. C., Walker, M. D., Miller, G. C., Ellison, T. A., Holsinger, L. D., Potter, J. L., Jackson, T. L., Chen, R. K., Winkel, V. L., Zhang, Z., McKinney, S., and de Crombrugghe, B. (2003) Adjacent DNA sequences modulate Sox9 transcriptional activation at paired Sox sites in three chondrocyte-specific enhancer elements. *Nucleic Acids Res.* **31,** 1541–1553
39. Arango, N. A., Lovell-Badge, R., and Behringer, R. R. (1999) Targeted mutagenesis of the endogenous mouse Mis gene promoter. *In vivo* definition of genetic pathways of vertebrate sexual development. *Cell* **99,** 409–419
40. De Santa Barbara, P., Bonneaud, N., Boizet, B., Desclozeaux, M., Moniot, B., Sudbeck, P., Scherer, G., Poulat, F., and Berta, P. (1998) Direct interaction of SRY-related protein SOX9 and steroidogenic factor 1 regulates transcription of the human anti-Müllerian hormone gene. *Mol. Cell. Biol.* **18,** 6653–6665
41. Wilhelm, D., Hiramatsu, R., Mizusaki, H., Widjaja, L., Combes, A. N., Kanai, Y., and Koopman, P. (2007) SOX9 regulates prostaglandin D synthase gene transcription *in vivo* to ensure testis development. *J. Biol. Chem.* **282,** 10553–10560

Pyoderma Gangrenosum With Wrist Joint Destruction: Case Report

Hyonmin Choe, MD, PhD, Hiroaki Sakano, MD, PhD, Hidetake Takigami, MD, PhD, Yutaka Inaba, MD, PhD, Kosuke Matsuo, MD, PhD, Tomoyuki Saito, MD, PhD

Pyoderma gangrenosum (PG) is a rare, noninfectious, neurotrophic dermatosis. We observed a case of PG mimicking cutaneous and osteoarticular infections that presented with a prolonged ulcer on the forearm, severe wrist pain, anemia, substantial local and systemic inflammation as evaluated by serum laboratory data, and carpal osteolysis. Although PG rarely damages joints, the ulcer extended to the joint and destroyed the osteochondral tissues. Advanced ulcerative colitis, which is a most common comorbidity of PG, proved to be an underlying disease. Antibiotic and surgical treatment did not heal the ulcer, which was successfully treated with corticosteroids. This intractable ulcer is often misdiagnosed. Hence when a patient presents with an enlarged, painful, unusual skin lesion, PG should always be considered. *(J Hand Surg 2013;38A:357–361.*

Key words Destructive change in wrist joint, noninfectious neutrophic dermatosis, pyoderma gangrenosum, ulcer, ulcerative colitis.

PYODERMA GANGRENOSUM (PG) is a noninfectious necrosis characterized by heavy neutrophil infiltration, engorged veins and capillaries, hemorrhage, and coagulation.[1,2] It typically begins as a pustule or vesiculopustule that progresses to an ulcer with undermined borders. Half of patients have an associated underlying systemic disease such as ulcerative colitis (UC), Crohn disease, rheumatoid arthritis, and other autoimmune diseases.[3,4] Thus, the awareness of the characteristic ulcer is also important for diagnosing the underlying disease.

Pathogenesis is still unknown, but heavy neutrophil infiltration is clearly relevant, and recent studies demonstrated increased expression of the pro-inflammatory cytokines in this disease.[5] Therefore, PG could possibly invade joints, and this has been reported for PAPA syndrome (pyogenic sterile arthritis, PG, and acne),[6–8] which is caused by the mutations of the gene.

We present a case of PG that was previously misdiagnosed as an infectious disease and, therefore, led to a prolonged skin ulcer, advanced UC, and destruction of the wrist joint.

CASE REPORT

The patient was a 60-year-old woman who complained of high fever, diarrhea, and anemia along with pain, swelling, and redness in the left wrist, without any previous history of skin ulcer or arthritis. The pain began with a small papule on the left forearm. The papule progressed to form a small ulcer. She first visited a hospital near her home where necrotizing fasciitis was suspected based on her white blood cell count of 15,600/μL and C-reactive protein level of 22.4 mg/dL. The necrotic tissue in the left forearm was debrided. Tissue samples were submitted for microbiological culture, but the result was negative. Despite these negative results, the antibiotic treatment was continued; nevertheless, a deep ulcer gradually formed on the dorsal forearm. The deep, large skin lesion was treated with

From the Department of Orthopaedic Surgery, Yokohama City University School of Medicine, Yokohama, Japan; Department of Orthopaedic Surgery, Hiratsuka Kyosai Hospital, Hiratsuka, Japan.

Received for publication July 6, 2012; accepted in revised form October 30, 2012.

No benefits in any form have been received or will be received related directly or indirectly to the subject of this article.

Corresponding author: Hyonmin Choe, MD, PhD, Department of Orthopaedic Surgery, Yokohama City University, 3-9 Fukuura, Kanazawa-ku, Yokohama City, Japan; e-mail: hyonmin@hotmail.com.

0363-5023/13/38A02-0019$36.00/0
http://dx.doi.org/10.1016/j.jhsa.2012.10.049

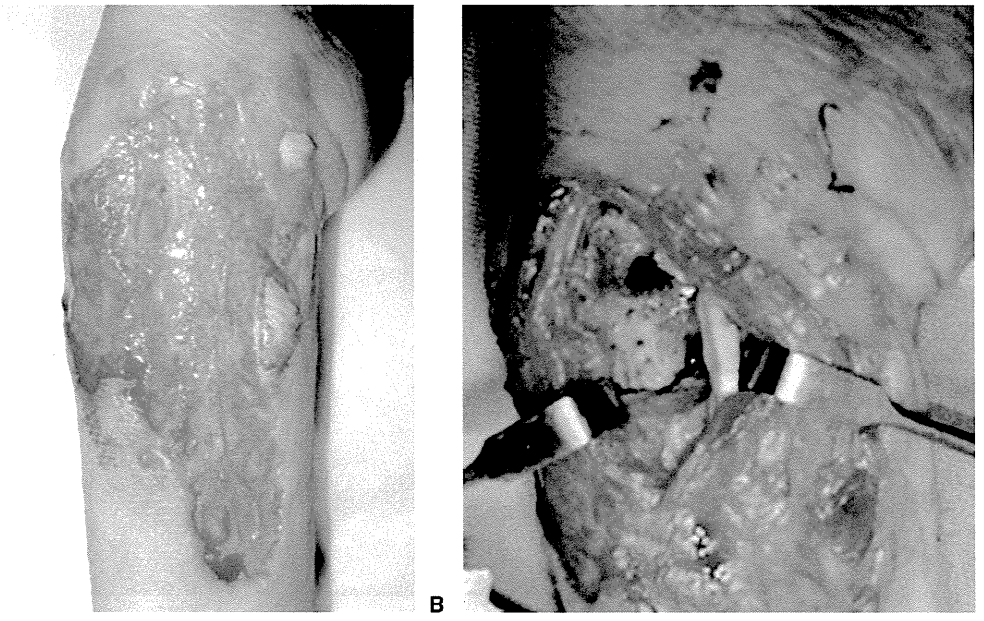

FIGURE 1: Ulcer on the palmar side of the left forearm. **A** Relapsed ulcer on the volar left forearm. **B** The ulcer had a violaceous border and extended into the radiocarpal joint.

dermal grafting, and her wound appeared to be epithelialized 2 months after the surgical procedure. Follow-up was discontinued, although high fever, wrist pain, and diarrhea persisted. In June 2007, she had an ulcer on her volar forearm with increased wrist pain.

On presentation to our hospital, the patient complained of general malaise, diarrhea, and severe pain in her left hand. Her white blood cell count was 11,400/ μL, and C-reactive protein level was 10.7 mg/dL. She was severely anemic, and her hemoglobin level was 3.4 g/dL. She was hospitalized immediately. The possibility of rheumatoid arthritis was excluded because laboratory data for rheumatoid factor were normal, and there was no arthritis in any other joint. She experienced persistent pain in the left wrist but not elsewhere. The ulcer had spread volarly with a violaceous border overhanging the ulcer bed (Fig. 1). In contrast to the normal X-ray findings at the previous hospital, current X-rays revealed destructive changes in the radioulnar and radiocarpal joints (Fig. 2A), and magnetic resonance imaging showed inflammation in the radiocarpal joint and in the trapezium (Fig. 2B). On the basis of clinical and radiological findings, we suspected chronic osteoarticular infection and performed surgical debridement. Although results of the microbiological culture were negative, histopathological findings showed infiltration of inflammatory cells into bone and soft tissues (Fig. 3), which is consistent with pyogenic infection, and antibiotics were administered. To identify the cause of anemia and diarrhea, a colonoscopy was also performed, and UC was diagnosed.

Daily administration of 40 mg corticosteroids for UC greatly improved the ulcer on the forearm. A few weeks later, the ulcer showed epithelialization (Fig. 4A), and pain in the wrist had been relieved. However, total colectomy was required to treat advanced UC, and loss of function in the wrist joint was unavoidable (Fig. 4B).

DISCUSSION

In 1908, Brocq reported a series of patients with typical features of the entity named PG in 1930 by Brunsting,[9,10] who believed that a bacterial infection was responsible for this intractable ulcer. The name *pyoderma gangrenosum* has persisted, although PG is currently characterized as noninfectious neurotrophic dermatosis.[11,12] The male/female distribution of PG is equal or with a slight female predominance. The patient's age is generally from 25 to 50 years, although all ages have been reported. [13] Pyoderma gangrenosum usually occurs on the legs, but it can be found anywhere. In 50% of the cases, PG is associated with underlying systemic diseases such as irritable bowel disease, rheumatoid arthritis, and hepatitis,[4,14] but PG has also been reported in healthy individuals.[15] This variant of distributions is one factor of the difficulty of diagnosing PG. Furthermore, PG occurs with minor trauma or surgery in some cases and often mimics a superficial or postoperative infection.[1,16–18]

Powell et al described 4 clinical variants of PG—ulcerative (classic), pustular, bullous, and vegetative.[19] Classic PG starts with sterile pustules or a small papule. The pustules or papules develop into a painful ulcer

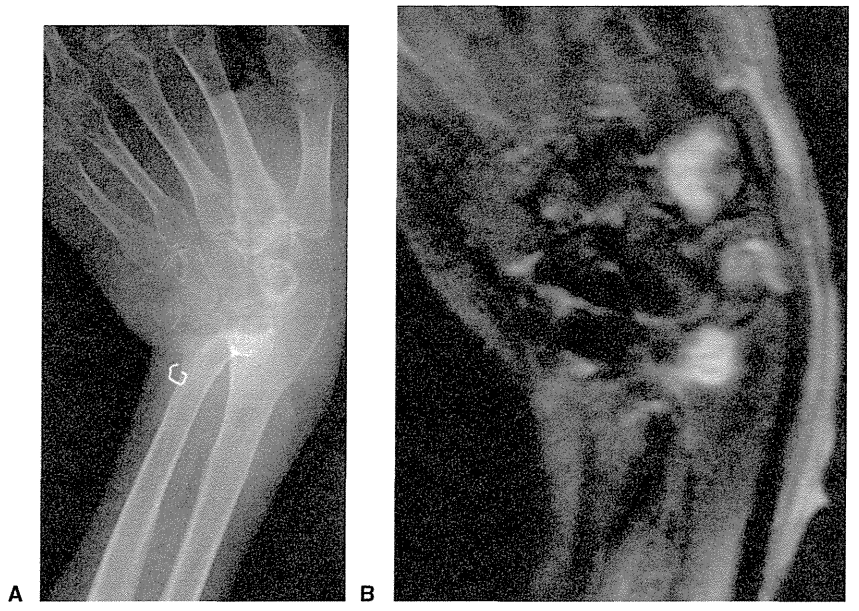

FIGURE 2: Images of the left hand. **A** X-ray of the wrist joint taken at our hospital shows destructive change in the radiocarpal, ulnocarpal, and midcarpal joints. **B** Magnetic resonance image of the left hand taken at our hospital shows inflammation in the radiocarpal joint and in the trapezium with high intensity in the T2-weighted image (with fat suppression).

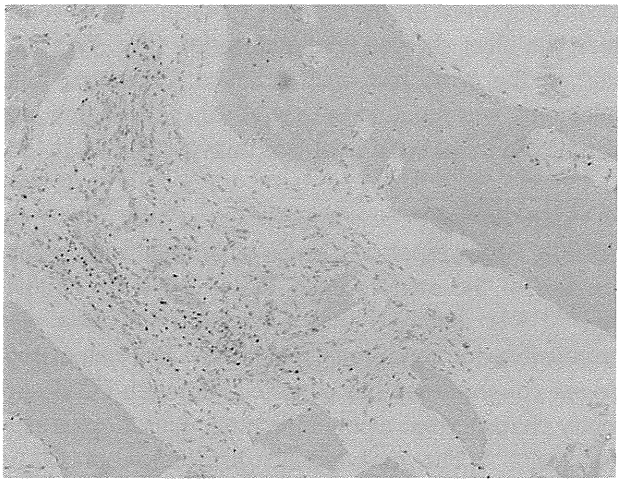

FIGURE 3: Histopathology of the ulcer on the palmar side of the left forearm. Histopathological finding shows infiltration of inflammatory cells including neutrophils (hematoxylin-eosin, original magnification × 100).

with indeterminate, violaceous borders.[2,20] Regardless of the characteristic morphology, diagnostic criteria for PG have not been universally accepted or validated because several variants of ulcer conditions have been observed at several stages.[1,4] Accordingly, diverse appearances and rareness make it especially difficult to definitively diagnose PG.

Diagnosis of PG is based on a history of typical clinical presentation, histopathology, an underling disease, and exclusion of other diseases that would lead to a similar appearance.[1,4,20] Although Su et al proposed diagnostic criteria for PG,[21] to a large extent, the diagnosis of PG is a diagnosis of exclusion.[11] Awareness of the typical features, including association with underlying disease, facilitates making the diagnosis. Careful deliberation and clinicopathologic exclusion of diseases of similar appearance are necessary. In addition, it is essential that PG should be on the list of diagnostic considerations when faced with a patient with unusual skin ulcerations. Therefore, it is important to know the characteristics of PG, which mimics several other diseases and is most commonly mistaken for the infection because of the inflammation and laboratory data.[14]

For differential diagnosis, early papules, nodules, or pustules must be examined for infection, including bacteria, fungal, mycobacterial, and viral, in addition to Sweet syndrome, Behçet sydrome, panniculitides, and cutaneous polyarteritis nodosa. In ulcerative and vegetative lesions, infections, vasculitis, and thrombophilic states, and malignancy must be excluded.[1] Tissue sampling or biopsy must be performed as atraumatically as possible, because it may provoke a pathergy that exacerbates the existing ulcer.

The administration of prednisolone is the most commonly used medication, at a dose of 0.5–2 mg/kg/day, but it should be tapered gradually over 4–6weeks while starting a steroid sparing agent.[11,16,22] Cyclosporine with 3–6 mg/kg/day can be another first-line agent in the treatment of PG.[12] Aggressive surgical debridement

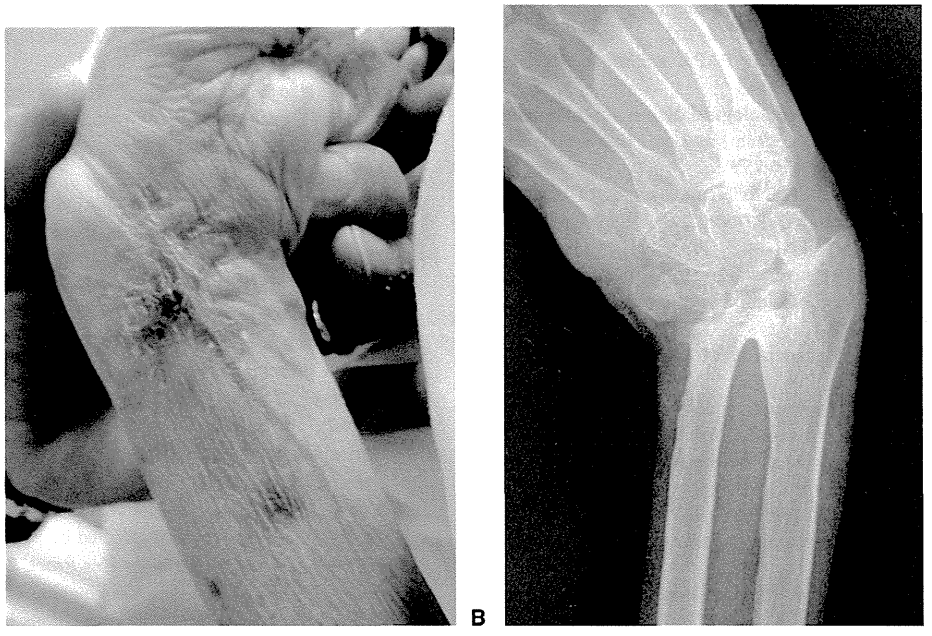

FIGURE 4: Images of the left forearm after administration of corticosteroids **A** Full epithelialization of the ulcer. **B** X-ray shows fusion of the distal radioulnar joint and radiocarpal joint.

of the lesion should be avoided because of disease progression secondary to pathergy. Moisture-retentive dressings appear to be suitable for reducing pain, inducing collagen production, facilitating autolytic debridement, and promoting angiogenesis.[2,12] Other multiple systemic and topical treatments (ie, tumor necrosis factor-alpha antagonists and hyperbaric oxygen) have been successfully used for the treatment of PG but are still challenges, because it is difficult to conduct large studies for this uncommon dermatosis.[11,12,20]

Joint deformities are known with PAPA syndrome,[6–8] which typically presents in children with recurrent polyarthritis; PG and acne are caused by the mutations of the gene. Our patient is unique because she had no PAPA syndrome, although her joint was destroyed by PG. Early diagnosis and treatment of PG are favorable to spontaneous healing without complex consequences. Diagnosis and treatment of PG was delayed in our case because the necrotic tissue and destructive changes in the wrist mimicked cutaneous and osteoarticular infection. Accordingly, the chronic ulcer enlarged to the depth of wrist, and PG progressed to joint destruction.

Histopathology is not specific in this disease because pathological findings of PG vary depending on the timing and the site of the biopsy.[2,20] However, lymphocytic or neutrophilic infiltrations are generally shown in an area of ulceration or in an erythematous border[2] and aberrant neutrophil trafficking has been proposed.[23] Furthermore, a recent study demonstrated increased expression of the pro-inflammatory cytokine interleukin-23 in PG patients.[5] Thus, prolonged invasion of inflammatory cells in the skin reached and destroyed osteochondral tissues, and this resulted in the wrist destruction in our case.

The importance and difficulty of diagnosing PG is shown by the present case. Because of the rareness and diverse pathogeneses of PG, the signs and symptoms were misinterpreted. Accordingly, prolonged joint inflammation and advanced UC resulted in a loss of wrist function and necessitated total colectomy. Early diagnosis and proper treatment could likely have hastened and improved the outcome. Surgical treatment and antibiotics were not effective, but corticosteroids were. Pyogenic gangrenosum must be considered when confronted with an enlarged, painful, unusual skin lesion, with or without destructive arthritis that mimics cutaneous and osteoarticular infection.

REFERENCES

1. Callen JP, Jackson JM. Pyoderma gangrenosum: an update. *Rheum Dis Clin North Am.* 2007;33(4):787–802.
2. Cohen PR. Neutrophilic dermatoses: a review of current treatment options. *Am J Clin Dermatol.* 2009;10(5):301–312.
3. Duarte AF, Nogueira A, Lisboa C, et al. Pyoderma gangrenosum—clinical, laboratory and therapeutic approaches. Review of 28 cases [in Portuguese]. *Dermatol Online J.* 2009;15(7):3.
4. Hadi A, Lebwohl M. Clinical features of pyoderma gangrenosum and current diagnostic trends. *J Am Acad Dermatol.* 2011;64(5):950–954.
5. Guenova E, Teske A, Fehrenbacher B, et al. Interleukin 23 expression in pyoderma gangrenosum and targeted therapy with ustekinumab. *Arch Dermatol.* 2011;147(10):1203–1205.
6. Samlaska CP, Smith RA, Myers JB, et al. Pyoderma gangrenosum and cranial osteolysis: case report and review of the paediatric literature. *Br J Dermatol.* 1995;133(6):972–977.
7. Demidowich AP, Freeman AF, Kuhns DB, et al. Brief report: genotype, phenotype, and clinical course in five patients with PAPA

syndrome (pyogenic sterile arthritis, pyoderma gangrenosum, and acne). *Arthritis Rheum.* 2012;64(6):2022–2027.
8. Tallon B, Corkill M. Peculiarities of PAPA syndrome. *Rheumatology (Oxford).* 2006;45(9):1140–1143.
9. Farhi D. The clinical and histopathological description of geometric phagedenism (pyoderma gangrenosum) by Louis Brocq one century ago. *Arch Dermatol.* 2008;144(6):755
10. Brunsting LA, Underwood LJ. Pyoderma vegetans in association with chronic ulcerative colitis. *Arch Derm Syphilol.* 1949;60(2):161–172.
11. Dabade TS, Davis MD. Diagnosis and treatment of the neutrophilic dermatoses (pyoderma gangrenosum, Sweet's syndrome). *Dermatol Ther.* 2012;24(2):273–284.
12. Schadt CR, Callen JP. Management of neutrophilic dermatoses. *Dermatol Ther.* 2012;25(2):158–172.
13. Bennett ML, Jackson JM, Jorizzo JL, et al. Pyoderma gangrenosum. A comparison of typical and atypical forms with an emphasis on time to remission. Case review of 86 patients from 2 institutions. *Medicine (Baltimore).* 2000;79(1):37–46.
14. Huish SB, de La Paz EM, Ellis PR III, et al. Pyoderma gangrenosum of the hand: a case series and review of the literature. *J Hand Surg Am.* 2001;26(4):679–685.
15. Rand RP, Olerud JE, Verrier ED. Pyoderma gangrenosum after coronary artery bypass grafting. *Ann Thorac Surg.* 1993;55(4): 1016–1018.
16. Armstrong PM, Ilyas I, Pandey R, Berendt AR, Conlon CP, Simpson AH. Pyoderma gangrenosum. A diagnosis not to be missed. *J Bone Joint Surg Br.* 1999;81(5):893–894.
17. Steenbrugge F, Raaijmaakers M, Caekebeke P, Van Landuyt K. Pyoderma gangrenosum following trauma of the knee: A case of pathergy and review of orthopaedic cases. *Injury.* 2010;42(4):421–423. Epub 2010 Jul 17.
18. Bennett CR, Brage ME, Mass DP. Pyoderma gangrenosum mimicking postoperative infection in the extremities. A report of two cases. *J Bone Joint Surg Am.* 1999;81(7):1013–1018.
19. Powell FC, Su WP, Perry HO. Pyoderma gangrenosum: classification and management. *J Am Acad Dermatol.* 1996;34(3):395–409.
20. Hasselmann DO, Bens G, Tilgen W, et al. Pyoderma gangrenosum: clinical presentation and outcome in 18 cases and review of the literature. *J Dtsch Dermatol Ges.* 2007;5(7):560–564.
21. Su WP, Davis MD, Weenig RH, et al. Pyoderma gangrenosum: clinicopathologic correlation and proposed diagnostic criteria. *Int J Dermatol.* 2004;43(11):790–800.
22. Richetta AG, D'Epiro S, Mattozzi C, et al. Folgoration as an example of pathergy in a patient affected by pyoderma gangrenosum and Takayasu's arteritis. *Dermatol Res Pract.* 2009;2009:393452.
23. Adachi Y, Kindzelskii AL, Cookingham G, et al. Aberrant neutrophil trafficking and metabolic oscillations in severe pyoderma gangrenosum. *J Invest Dermatol.* 1998;111(2):259–268.

Diagnostic Microbiology and Infectious Disease 74 (2012) 125–130

Contents lists available at SciVerse ScienceDirect

Diagnostic Microbiology and Infectious Disease

journal homepage: www.elsevier.com/locate/diagmicrobio

Quantitative evaluation of periprosthetic infection by real-time polymerase chain reaction: a comparison with conventional methods☆,☆☆

Yushi Miyamae *, Yutaka Inaba *, Naomi Kobayashi, Hyonmin Choe, Hiroyuki Ike, Takako Momose, Shusuke Fujiwara, Tomoyuki Saito

Department of Orthopaedic Surgery, Yokohama City University, School of Medicine, 3-9 Fukuura, Kanazawa-ku, Yokohama, Japan

ARTICLE INFO

Article history:
Received 9 March 2012
Accepted 18 June 2012
Available online 24 July 2012

Keywords:
Real-time PCR
Quantification
Periprosthetic infection

ABSTRACT

Several recent studies have demonstrated the limited accuracy of conventional culture methods for diagnosing periprosthetic infections. We have applied real-time polymerase chain reaction (PCR) assays for the rapid identification of bacteria around implants and reported its utility. However, the capability of quantification is also a useful feature of this type of assay. The aim of our study was to validate the usefulness of quantitative analyses using real-time PCR of cases with clinical periprosthetic infections in comparison with more established tests, such as C-reactive protein (CRP) levels, microbiologic cultures, and histopathology. Fifty-six joints with suspected infections were reviewed retrospectively. A universal PCR assay was used to perform the quantitative analyses. The differences in the threshold cycles between clinical samples and a negative control (ΔCt) in each case were calculated. The results of the quantitative PCR assay were compared with CRP levels, microbiologic cultures, and histopathology. There was a significant correlation found between the CRP and ΔCt values. There were also significant differences found in the ΔCt values according to CRP levels, with higher CRP levels showing higher ΔCt values. Similarly, there were significant differences in the ΔCt measurements in our culture results and among our pathologic evaluations. We confirmed that quantification by universal PCR based on the ΔCt correlated with preoperative CRP levels and was associated with the microbiologic culture results and pathologic severity. This quantification method may be valuable for assessing infection severity.

1. Introduction

Total joint arthroplasty is commonly recognized as the most effective treatment for osteoarthritis and rheumatoid arthritis, and this procedure has been improved over the years in terms of the implant design, more stable long-term clinical results, and a reduced frequency of complications. Despite these improvements, however, periprosthetic infection remains a serious potential complication of joint arthroplasty. Difficulties have occurred in the detection of such infections with conventional culture methods, and several recent studies have demonstrated the limited accuracy of this approach for diagnosing periprosthetic infections, particularly low-grade infections that often cause false-negative results (Kobayashi et al., 2008; Tunney et al., 1999). No single laboratory test has sufficient sensitivity or specificity for diagnosing such low-grade infections (Bare et al., 2006). Histopathologic evaluations are thought to be the most reliable tests for diagnosing bacterial infections because of their high specificity, but previous reports have indicated that intraoperative analyses using frozen sections have poor sensitivity in this regard (Della Valle et al., 1999; Kanner et al., 2008). Hence, the diagnosis of periprosthetic infections remains a challenge for clinicians and requires an evaluation with several different tests in parallel.

A number of molecular diagnostic tests have recently been developed for detecting microbial infections. Most are polymerase chain reaction (PCR) based and have been reported to be effective in cases of respiratory (Peters et al., 2009; Yang et al., 2005), neurologic (Darton et al., 2009; Hackett et al., 2002; Kearns et al., 1999), and pediatric (Chen et al., 2004; Perkins et al., 2005) infections, which are of a viral or bacterial nature. In addition, several previous studies have demonstrated the usefulness of PCR-based assays for the detection of periprosthetic bacterial infections in an orthopedic setting (Clarke et al., 2004; Mariani et al., 1996; Tarkin et al., 2003). Notably, the rapid and sensitive real-time PCR technique is increasingly being recognized as an alternative tool for diagnostic testing (Mackay, 2004). In addition, we previously employed and reported the utility of a real-time PCR assay for the detection of periprosthetic infections, particularly as an intraoperative identification tool, due to its extreme rapidity and ability to specifically identify methicillin

☆ Funding: No financial support has been received for this work.
☆☆ Conflicts of interest: None for all authors.
* Corresponding authors. Yutaka Inaba is to be contacted at Tel.: +81-787-2655; fax: +81-781-7922. Yushi Miyamae, Tel.: +81-787-2655; fax: +81-781-7922.
E-mail addresses: yushimiyamae@yahoo.co.jp (Y. Miyamae), yute0131@med.yokohama-cu.ac.jp (Y. Inaba).

0732-8893/$ – see front matter © 2012 Elsevier Inc. All rights reserved.
doi:10.1016/j.diagmicrobio.2012.06.017

resistance (Kobayashi et al., 2009a). However, although the quantification capability of real-time PCR is a useful feature of this detection method, there have been few previous studies that have evaluated its utility in comparison with other diagnostic tests.

The aim of our present study was to validate the usefulness of quantitative analyses using real-time PCR of clinical periprosthetic infection cases in comparison with more established tests, such as serologic evaluations of C-reactive protein (CRP) levels, microbiologic culture, and histopathology.

2. Methods

2.1. Patients

This study was approved by our institutional review board. From January 2007 to April 2010, a total of 38 cases, which involved 56 joints including 41 hip joints (12 one-stage revision arthroplasty, 16 two-stage revision arthroplasty, and 13 implant removal), 11 knee joints (5 two-stage revision arthroplasty, 3 implant removal, and 3 hydroxyapatite block replacement), and 4 debridement joints of suspected infection or aseptic loosening that had undergone surgery were enrolled to this study. Fourteen patients were treated by antibiotics within a week of the surgical procedure. Intraoperative real-time PCR assays were performed for all cases, and quantitative evaluation was reviewed retrospectively. The CRP levels were measured prior to each operation in all cases, and intraoperatively collected tissue samples were evaluated by microbiologic culture and histopathology. As the underlying inflammatory conditions, 1 patient had rheumatoid arthritis and 2 patients had malignant tumor (osteosarcoma and pancreatic carcinoma).

2.2. Real-time PCR

Intraoperative real-time PCR assays were performed as described previously (Kobayashi et al., 2009a). Briefly, for manual DNA extraction from samples, we performed ultrasonication (Bransonic 2510 Ultrasonic cleaner; Branson Ultrasonics, Danbury, CT, USA) at a frequency of 40 kHz for 5 min using a plastic bag and 1 mL of sterile water. The sonicated solutions were collected and then applied to a DNA purification column (QIAamp DNA Mini Kit; QIAGEN, Hilden, Germany). A universal PCR assay with a LightCycler® system (Roche Diagnostics Corporation, Indianapolis, IN, USA) that targets the 16S rRNA gene was used for the quantitative analysis. Differences in the threshold cycles between the clinical samples and a negative control (ΔCt) were calculated in each case based on the LightCycler quantification mode.

2.3. C-Reactive protein

As a serologic marker of inflammation, the CRP levels (mg/dL) were reviewed in each case, and the patients were accordingly divided into the following 3 groups: CRP < 0.2 mg/dL, 0.2 mg/dL ≤ CRP ≤ 1 mg/dL, and CRP > 1 mg/dL.

2.4. Microbiologic culture

All specimens were analyzed with standard microbiologic cultures with a direct plating method and broth medium, conducted on both blood agar and Gifu anaerobic medium agar simultaneously. The results were reviewed, and the samples were divided into 3 groups based on the following results: negative, positive (under enrichment culture conditions with Gifu anaerobic medium agar), and strongly positive (under normal culture conditions with blood agar). Briefly, Gifu anaerobic medium agar, which has high nutrient condition enough for anaerobes to grow, was developed for anaerobic bacterial growth of a wide range. Some organisms that grew in blood agar sooner were sent for a Gram stain and then, according to the result, added to the appropriate agar, and, finally, the grown-up organisms represented strong positive result. On the other hand, after incubation in anaerobic jars containing hydrogen and carbon dioxide generators at 35 °C for 5 days, some organisms that grew in Gifu anaerobic medium agar represented positive result.

2.5. Histopathologic evaluation

Histopathologic evaluations of all specimens were performed intraoperatively using frozen sections and postoperatively using permanent preparations. Histopathologic findings were reviewed, and the samples were divided into the following 3 groups based on the level of neutrophil infiltration that was determined under a high-power field (HPF, 400×): negative (no neutrophil), positive (minimum of 1 HPF containing 1–10 neutrophils), and strongly positive (minimum of 5 HPF containing 10 or more neutrophils).

2.6. Definition of infection

We defined a result as an infection if strongly positive results were obtained with microbiologic culture, pathologic findings, or both.

2.7. Clinical evaluations

The average follow-up period was 14.2 months (range, 1–36). At the final follow-up examination, the existence of a radiolucent line or any other evidence of implant loosening was evaluated on an anteroposterior and lateral view by plain X-ray, and CRP values were evaluated serologically.

2.8. Statistics

The correlation between ΔCt and CRP value was analyzed by Pearson's correlation. The differences in the ΔCt values in each group were evaluated using the Kruskal–Wallis test and 1-way factorial analysis of variance followed by a post-hoc test using Fisher's protected least significant difference test. Analyses of receiver operating characteristic (ROC) curves for ΔCt for infection were then performed.

3. Results

In the evaluations of the preoperative CRP levels, there were 27 cases with CRP levels of less than 0.2, 14 cases with CRP levels between 0.2 and 1.0, and 15 cases with CRP levels higher than 1.0 among our study cohort. The culture results indicated 41 negative, 8 positive, and 7 strongly positive cases. In our pathologic evaluations, there were 15 negative, 26 positive, and 15 strongly positive findings. There was a significant correlation found between the preoperative CRP levels and ΔCt values (Fig. 1; $r = 0.54$, $P < 0.01$). There were also significant differences found in the ΔCt for each group divided by the preoperative CRP level, with higher CRP levels showing higher ΔCt values (Fig. 2). Similarly, there were significant differences in the ΔCt measurements among the groups divided by our culture results and among those divided by our pathologic evaluations. In the culture tests, there were significant differences detected between the negative and strongly positive ($P < 0.01$) and between the positive and strongly positive groups ($P < 0.01$) (Fig. 3). In terms of the pathologic results, significant differences were found between the negative and strongly positive ($P < 0.01$) and between the positive and strongly positive groups ($P < 0.01$) (Fig. 4). ROC curves revealed that the sensitivity and specificity of PCR with a ΔCt cut-off at 1.9 cycles were 94% and 51%, respectively.

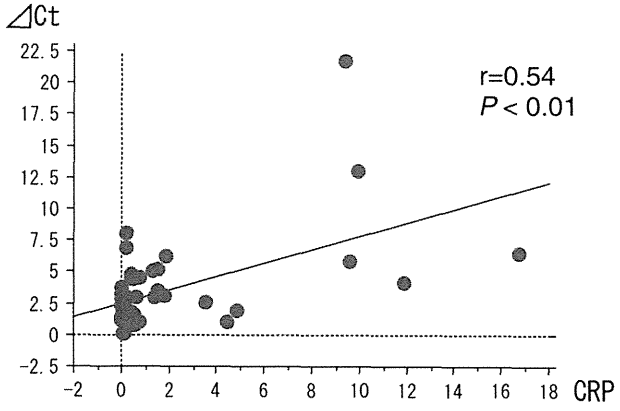

Fig. 1. Correlation between the differences in threshold cycles between the clinical samples and a negative control (ΔCt) value and the C-reactive protein (CRP) levels. There was a significant correlation found between the CRP levels and ΔCt values ($r = 0.54$, $P < 0.01$).

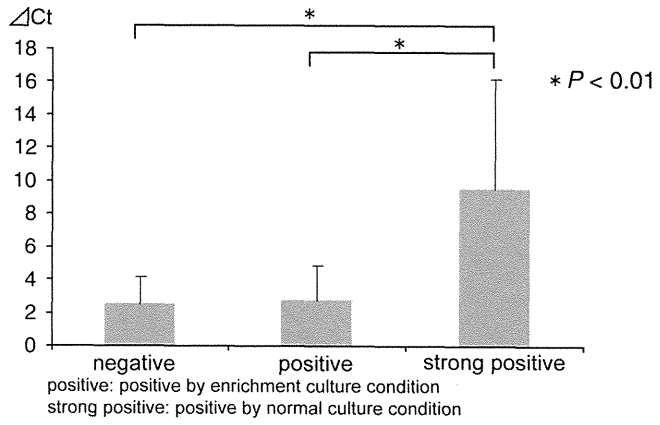

Fig. 3. Differences in ΔCt values among the patients grouped by culture results. Among the groups divided by culture results, there were significant differences between the negative and strongly positive ($P < 0.01$) and between the positive and strongly positive groups ($P < 0.01$).

3.1. Clinical evaluation

We found that all 38 cases had been followed continuously, but that 2 patients were not evaluated in this way as they had died from either a medical complication or an unknown cause. At the last follow-up examination, there were 14 cases with CRP levels between 0.2 and 1.0, and 5 cases with CRP levels higher than 1.0. The remaining 17 cases had CRP levels that were less than 0.2. Radiologically, 4 cases exhibited radiolucent lines around the acetabular components at the last follow-up examination, and 3 had radiolucent lines that were 2 mm wide or less. However, no loosening or further progression was observed in these 3 patients, while the other patient had a radiolucent line that was more than 5 mm wide that had been earmarked for revision surgery on the suspicion of reinfection. No cases with a radiolucent line around the stem were observed. One of the patients without a radiolucent line required a cup revision because of a traumatic dislocation and the implant coming off the acetabulum.

Fig. 5 shows the real-time PCR quantification of a representative case. In this patient, the CRP value before the procedure was 0.41 (mg/dL), and intraoperative histopathologic findings showed several neutrophils. We could not diagnose as infection confidently with the results of these tests. Then we analyzed tissue samples around the implant in this patient using real-time PCR and calculated a ΔCt of 4.81 intraoperatively. Based on the result of real-time PCR, we considered the patient with a periprosthetic infection and performed an implant removal for this case. Several days after implant removal, the tissue culturing consistently revealed a Gram-positive bacillus. After a waiting period of 3 months, a 2-stage revision was performed upon the intraoperative confirmation of a negative result by real-time PCR. Fig. 6 shows the results of another representative case with an infection that was diagnosed by intraoperative real-time PCR. In this patient, the CRP value before the procedure was 16.78 (mg/dL). The PCR analysis revealed an infection with a Gram-positive species and a high ΔCt of 6.43. We performed a joint implant removal during which we applied our intraoperative histopathologic findings that showed an abundance of neutrophils. In addition, cultures of the aspiration sample produced methicillin-sensitive *Staphylococcus aureus* several days after the implant removal.

4. Discussion

Several previous reports have demonstrated the usefulness of PCR-based assays for the detection and quantification of viral or bacterial infections (Darton et al., 2009; Hackett et al., 2002; Kearns et al., 1999; Perkins et al., 2005; Peters et al., 2009; Yang et al., 2005). Although the application of PCR to quantitative assessments seems to be better developed for some infectious diseases and certain types of viral infection, there have been no studies to date that have validated the quantifiability of PCR for periprosthetic infections.

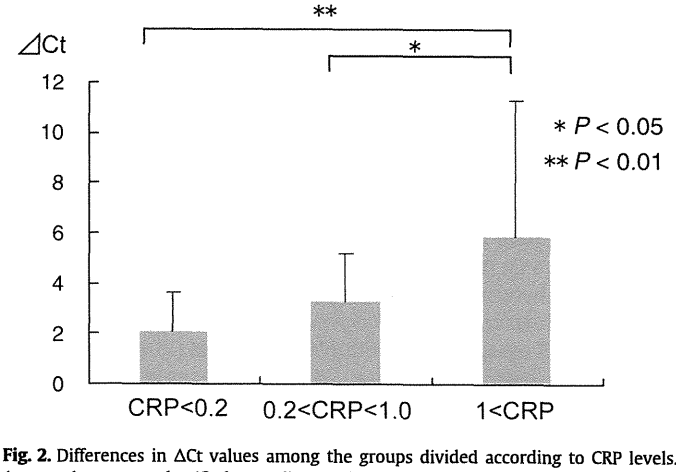

Fig. 2. Differences in ΔCt values among the groups divided according to CRP levels. Among the groups classified according to their preoperative CRP levels, there was a significant difference in the ΔCt values between the CRP <0.2 and CRP >1.0 groups ($P < 0.01$).

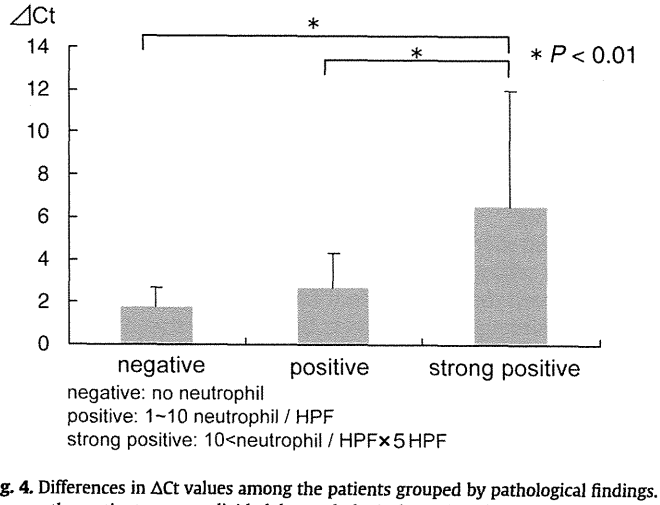

Fig. 4. Differences in ΔCt values among the patients grouped by pathological findings. Among the patient groups divided by pathological results, there were significant differences between the negative and strongly positive ($P < 0.01$) and between the positive and strongly positive ($P < 0.01$) groups.

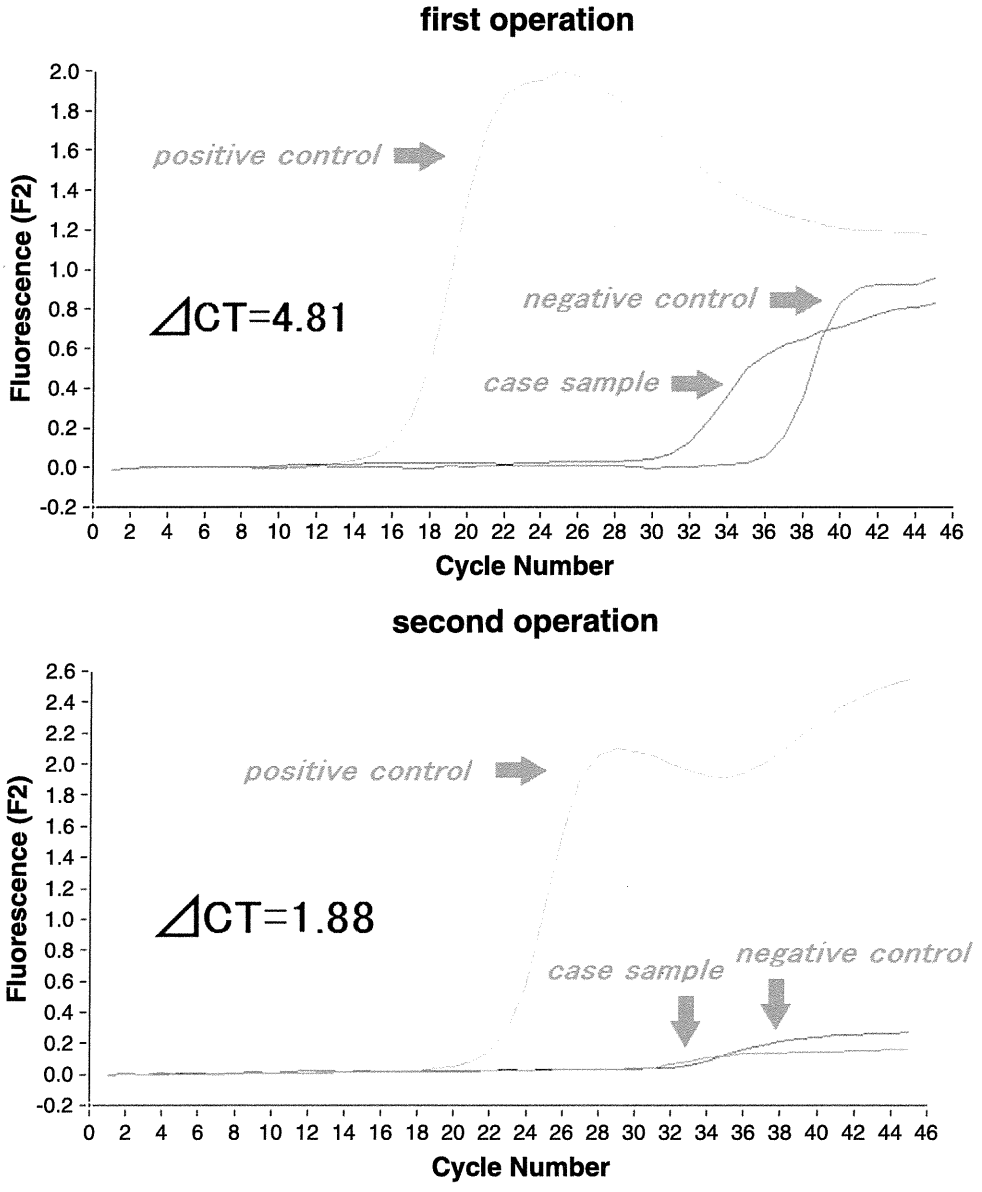

Fig. 5. Real-time polymerase chain reaction (PCR) quantification results from a representative 2-stage revision case. At the first operation, this patient showed a positive result after around 31 cycles of PCR, whilst the positive and negative control were positive after about 14 and 36 cycles, respectively. In this case, the ΔCt was calculated as 4.81. At the second operation, this decreased to 1.88, indicating a reduced level of bacterial DNA.

Hence, our current report is the first study to validate the use of real-time PCR for the quantitative evaluation and diagnosis of periprosthetic infections in clinical samples and compare this method with other tests. We confirmed that quantification by universal PCR based on the ΔCt value correlated with the preoperative CRP values and was associated with the microbiologic culture results and pathologic severity.

In the field of orthopedics, PCR assays have now been compared in a number of settings with conventional microbiologic cultures, which have long been the gold standard for the diagnosis of periprosthetic infections. Although some reports have demonstrated that PCR was not superior to microbiologic culture (Ince et al., 2004), the majority of studies on this issue have emphasized the usefulness of PCR-based techniques for the diagnosis of periprosthetic bacterial infections (Clarke et al., 2004; Mariani et al., 1996; Tarkin et al., 2003; Tunney et al., 1999). For example, Tunney et al. (1999) reported that the prevalence of infection around prosthetic joints might be underestimated by conventional tests. They utilized ultrasonication to dislodge any biofilm around total joint implants and then employed a 16S rRNA universal PCR assay for the detection of bacterial DNA. A much higher detection of occult infection was found with this technique compared with conventional cultures. We have also previously described the usefulness of the intraoperative identification of bacterial DNA by PCR to detect periprosthetic infections and reported a comparatively high specificity of 80% in clinical use (Kobayashi et al., 2009a), even though PCR has been generally recognized in the past to have a poor specificity (Clarke et al., 2004).

Over the past decades, previous studies have suggested that conventional PCR testing is unreliable because of its inability to discriminate between colonization and infection. To overcome this problem, there have been several previous studies that have validated the use of PCR assays for quantitative evaluations (Chen et al., 2004; Darton et al., 2009; Hackett et al., 2002; Perkins et al., 2005; Peters et al., 2009; Yang et al., 2005). Yang et al. (2005) were the first to report the clinical utility of a quantitative PCR assay in diagnosing pneumonia and demonstrated that using this test with sputum samples can detect *Streptococcus pneumoniae* in adult patients with community-acquired pneumonia. Peters et al. (2009), who only

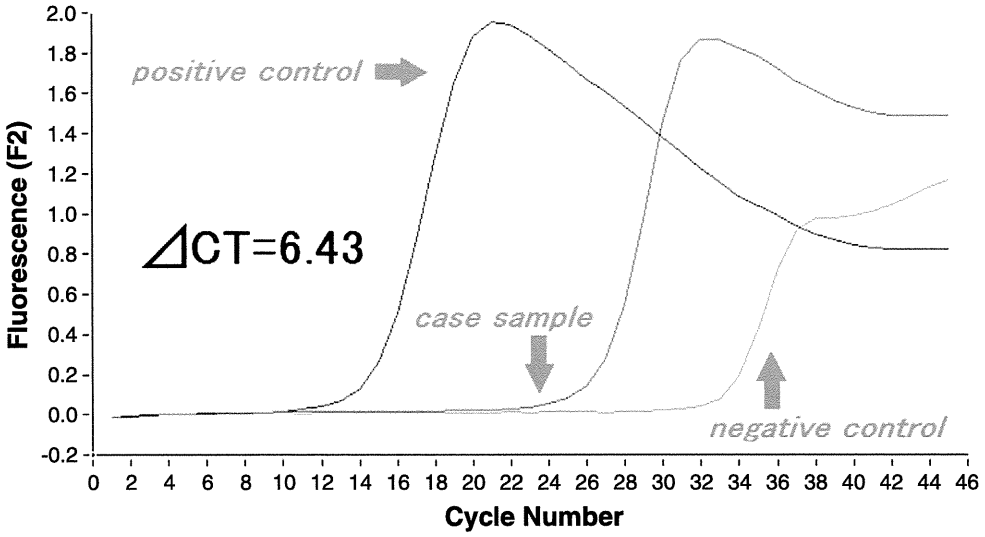

Fig. 6. Quantification results from a representative case of infection diagnosed by intraoperative real-time PCR. This patient showed a positive PCR result after around 26 cycles, while the negative control showed positivity after about 33 cycles. The ΔCt value was thus calculated as 6.43.

validated the usefulness of quantitative analyses using real-time PCR in comparison with more established laboratory tests, reported that the quantification of bacteria using PCR has a higher positive predictive value than the CRP levels or white blood cell (WBC) counts in patients with community-acquired pneumonia and that positive correlations could be observed for the quantification of bacteria based on the WBC counts, CRP levels, and length of stay. These authors evaluated the bacterial DNA load (BDL) as a diagnostic tool and demonstrated that this was related to both clinical and laboratory parameters, including CRP levels and WBC counts. They further confirmed that measuring the BDL not only supported the diagnosis of pneumonia but also provided a marker for the severity of this disease. In our current study, quantification by PCR using the ΔCt, whose method was demonstrated in a previous in vivo study (Corless et al., 2000) and which we use in clinical use, was found to correlate with the preoperative CRP levels.

In a clinical setting, occasional cases arise that show borderline characteristics with both preoperative CRP levels and intraoperative pathologic findings. In such instances, quantitative evaluations by intraoperative real-time PCR should provide useful supplemental information that may suggest suspicious infections. For example, the possibility of infection is regarded as relatively low in cases with a ΔCt under 1.9, and this resulted in a sensitivity of 94% and a specificity of 51%, as determined by universal PCR. In contrast, we can suspect infection more strongly in cases with a ΔCt higher than 1.9 as we have shown in our case example. A noteworthy issue in relation to the use of a PCR assay is the existence of PCR-positive, but culture-negative, cases, which may sometimes be false positives. Over the past decade, PCR has been recognized as a highly sensitive method that can detect low-grade infections that cannot be cultured, and it debuted as a technique with poor specificity at this sensitivity level, raising the issue of possible contamination (Clarke et al., 2004; Corless et al., 2000; Kobayashi et al., 2008). The universal PCR assays we used in our present analyses were based on the 16S rRNA gene and can be subject to contamination through the use of some commercially available Taq polymerase reagents that contain traces of *Escherichia coli* DNA, which is the bacterial system used to produce the enzyme as a recombinant protein (Corless et al., 2000). In PCR-positive but culture-negative cases, however, quantification by PCR can be considered to be a robust way of validating infection. This is because a higher ΔCt, which means a higher amount of bacterial DNA, suggests the clear existence of infection despite a negative culture result. In contrast, a lower ΔCt, which means a lower amount of bacterial DNA, suggests the possibility of a false positive due to contamination. Therefore, in a clinical setting also, we actually selected 2-stage revision surgery after implant removal and a waiting period in the case with PCR-positive (with ΔCt higher than 1.9) but culture-negative result. It is not described in this article, but we also evaluated melting peak analysis in real-time PCR, which enables us to distinguish whether bacterial DNA was from Gram-positive or Gram-negative species as described in a previous study (Kobayashi et al., 2009a).

Another issue to consider is the inability to confirm the viability of bacteria in PCR-positive cases. PCR can detect bacterial DNA from both viable and necrotic organisms, such that traces of only a few necrotic bacteria that have been dislodged from an implant surface may yield a false-positive PCR result (Kobayashi et al., 2009b). In an attempt to overcome this problem, Birmingham et al. (2008) reported the possibility of using reverse transcription-PCR to detect only live bacteria as necrotic organisms do not produce mRNA. In addition, Kobayashi et al. (2009b) investigated the use of propidium monoazide (PMA) to differentiate viable from dead bacteria. PMA has been used as a DNA-binding agent for differentiating intact from membrane-compromised bacterial cells and thus has the ability to penetrate dead bacterial cells with compromised membranes. Although we demonstrated the relationship between ΔCt and the other tests in the current study, this issue should be addressed in a future study.

One of the limitations of our present study was related to the method of quantification by real-time PCR. We simply calculated the difference in the crossing point between the samples and a negative control and represented this as the ΔCt. Hence, we did not quantify the actual total amount of amplified DNA in comparison with reference control samples. Nevertheless, we detected a relationship between these ΔCt measurements and the results of other tests that indicated that our simple PCR-based method has utility for routine clinical use. Another limitation was that we have to consider the influence of antibiotics on the results. In our present study, 14 patients were treated by antibiotics within a week of the surgical procedure. The antibiotics treatment possibly affected the results of the microbiologic culture and also the PCR results. In addition, we have to consider the effects of some underlying inflammatory conditions such as rheumatoid arthritis. In the current series, we included 1 case of rheumatoid arthritis and 2 cases of malignant tumor, which might have influenced the results of CRP and histopathology.

In conclusion, we demonstrated that quantitative evaluations by real-time PCR in conjunction with other tests have potential value for

assessing cases with possible periprosthetic infections. The quantification advantages of this PCR method may provide supplemental information for determining the severity of the infection. Additional studies are needed with more clinical cases to further validate this methodology.

Acknowledgment

The authors thank a laboratory technician, Kimi Ishikawa, for performing the real-time PCR procedure and for the management of the LightCycler system.

References

Bare J, MacDonald SJ, Bourne RB. Preoperative evaluations in revision total knee arthroplasty. Clin Orthop Relat Res 2006;446:40–4.

Birmingham P, Helm JM, Manner PA, Tuan RS. Simulated joint infection assessment by rapid detection of live bacteria with real-time reverse transcription polymerase chain reaction. J Bone Joint Surg Am 2008;90(3):602–8.

Chen FH, Samson KT, Chen H, et al. Clinical applications of real-time PCR for diagnosis and treatment of human cytomegalovirus infection in children. Pediatr Allergy Immunol 2004;15(3):210–5.

Clarke MT, Roberts CP, Lee PT, Gray J, Keene GS, Rushton N. Polymerase chain reaction can detect bacterial DNA in aseptically loose total hip arthroplasties. Clin Orthop Relat Res 2004;427:132–7.

Corless CE, Guiver M, Borrow R, Edwards-Jones V, Kaczmarski EB, Fox AJ. Contamination and sensitivity issues with a real-time universal 16S rRNA PCR. J Clin Microbiol 2000;38(5):1747–52.

Darton T, Guiver M, Naylor S, et al. Severity of meningococcal disease associated with genomic bacterial load. Clin Infect Dis 2009;48(5):587–94.

Della Valle CJ, Bogner E, Desai P, et al. Analysis of frozen sections of intraoperative specimens obtained at the time of reoperation after hip or knee resection arthroplasty for the treatment of infection. J Bone Joint Surg Am 1999;81(5):684–9.

Hackett SJ, Guiver M, Marsh J, et al. Meningococcal bacterial DNA load at presentation correlates with disease severity. Arch Dis Child 2002;86(1):44–6.

Ince A, Rupp J, Frommelt L, Katzer A, Gille J, Lohr JF. Is "aseptic" loosening of the prosthetic cup after total hip replacement due to nonculturable bacterial pathogens in patients with low-grade infection? Clin Infect Dis 2004;39(11):1599–603.

Kanner WA, Saleh KJ, Frierson Jr HF. Reassessment of the usefulness of frozen section analysis for hip and knee joint revisions. Am J Clin Pathol 2008;130(3):363–8.

Kearns AM, Freeman R, Murphy OM, Seiders PR, Steward M, Wheeler J. Rapid PCR-based detection of *Streptococcus pneumoniae* DNA in cerebrospinal fluid. J Clin Microbiol 1999;37(10):3434.

Kobayashi N, Inaba Y, Choe H, et al. Simultaneous intraoperative detection of methicillin-resistant *Staphylococcus* and pan-bacterial infection during revision surgery: use of simple DNA release by ultrasonication and real-time polymerase chain reaction. J Bone Joint Surg Am 2009a;91(12):2896–902.

Kobayashi H, Oethinger M, Tuohy MJ, Hall GS, Bauer TW. Improving clinical significance of PCR: use of propidium monoazide to distinguish viable from dead *Staphylococcus aureus* and *Staphylococcus epidermidis*. J Orthop Res 2009b;27(9):1243–7.

Kobayashi N, Procop GW, Krebs V, Kobayashi H, Bauer TW. Molecular identification of bacteria from aseptically loose implants. Clin Orthop Relat Res 2008;466(7):1716–25.

Mackay IM. Real-time PCR in the microbiology laboratory. Clin Microbiol Infect 2004;10(3):190–212.

Mariani BD, Martin DS, Levine MJ, Booth Jr RE, Tuan RS. The Coventry Award. Polymerase chain reaction detection of bacterial infection in total knee arthroplasty. Clin Orthop Relat Res 1996;331:11–22.

Perkins SM, Webb DL, Torrance SA, et al. Comparison of a real-time reverse transcriptase PCR assay and a culture technique for quantitative assessment of viral load in children naturally infected with respiratory syncytial virus. J Clin Microbiol 2005;43(5):2356–62.

Peters RP, de Boer RF, Schuurman T, et al. *Streptococcus pneumoniae* DNA load in blood as a marker of infection in patients with community-acquired pneumonia. J Clin Microbiol 2009;47(10):3308–12.

Tarkin IS, Henry TJ, Fey PI, Iwen PC, Hinrichs SH, Garvin KL. PCR rapidly detects methicillin-resistant staphylococci periprosthetic infection. Clin Orthop Relat Res 2003;414:89–94.

Tunney MM, Patrick S, Curran MD, et al. Detection of prosthetic hip infection at revision arthroplasty by immunofluorescence microscopy and PCR amplification of the bacterial 16S rRNA gene. J Clin Microbiol 1999;37(10):3281–90.

Yang S, Lin S, Khalil A, et al. Quantitative PCR assay using sputum samples for rapid diagnosis of pneumococcal pneumonia in adult emergency department patients. J Clin Microbiol 2005;43(7):3221–6.